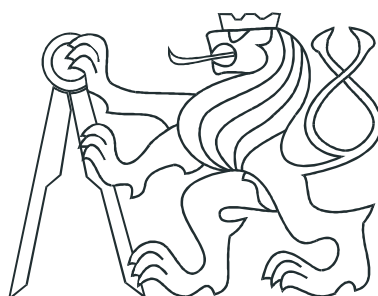# CZECH TECHNICAL UNIVERSITY IN PRAGUE

Faculty of Nuclear Sciences and Physical Engineering

Department of Physics



# Master's thesis

## Effect of beam non-factorisation on luminosity determination in ALICE experiment
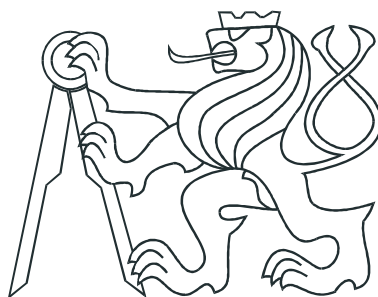
**Bc. Jan Půček**

**Supervisor: doc. Jesús Guillermo Contreras Nuño, PhD.**

**Prague, 2019**

ČESKÉ VYSOKÉ UČENÍ TECHNICKÉ
V PRAZE
Fakulta Jaderná a Fyzikálně Inženýrská
Katedra Fyziky



# Diplomová práce

## Vliv nefaktorizovatelnosti svazku na stanovení luminozity v experimentu ALICE

**Bc. Jan Půček**

Školitel: doc. Jesús Guillermo Contreras Nuño, PhD.

**Praha, 2019**

ČESKÉ VYSOKÉ UČENÍ TECHNICKÉ V PRAZE
**FAKULTA JADERNÁ A FYZIKÁLNĚ INŽENÝRSKÁ**
PRAHA 1 - STARÉ MĚSTO, BŘEHOVÁ 7 - PSČ 115 19

*Katedra:* fyziky                                    *Akademický rok:* 2018/2019

# ZADÁNÍ DIPLOMOVÉ PRÁCE

*Student:*                    Bc. Jan Půček

*Studijní program:*      Aplikace přírodních věd

*Obor:*                       Experimentální jaderná a částicová fyzika

*Název práce:*            Vliv nefaktorizovatelnosti svazku na stanovení luminozity v
*(česky)*                     experimentu ALICE

*Název práce:*            Effect of beam non-factorisation on luminosity determination in ALICE
*(anglicky)*                 experiment

*Pokyny pro vypracování:*

1) Zpracujte rešerši na téma luminozita a metody jejího určení na ALICE
2) Simulujte korekci vdM skenu pro korelované svazky a určete její neurčitost

*Doporučená literatura:*

[1] S. van der Meer: Calibration of the Effective Beam Height in the ISR, CERN-ISR-PO-68-31 (1968)

[2] R. Aaij, et al.: Precision luminosity measurements at LHCb, JINST 9, P12005 (2014)

[3] B. Abelev, et al.: Measurement of visible cross sections in proton-lead collisions at sqrt(s_NN) = 5.02 TeV in van der Meer scans with the ALICE detector, JINST 9, P11003 (2014)

[4] M. Aaboud, et al.: Luminosity determination in pp collisions at sqrt(s) = 8 TeV using the ATLAS detector at the LHC, The European Physical Journal C 76, 653 (2016)

[5] CMS Collaboration: CMS luminosity measurement for the 2015 data-taking period, Technical Report CMS-PAS-LUM-15-001 (2017)
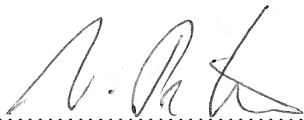
*Jméno a pracoviště vedoucího diplomové práce:*

doc. Jesús Guillermo Contreras Nuno, PhD., Katedra fyziky, Fakulta jaderná a fyzikálně inženýrská ČVUT v Praze

*Datum zadání diplomové práce:*     22.10.2018
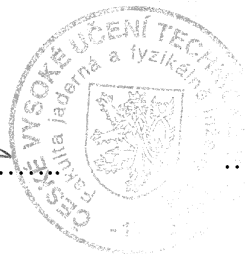
*Termín odevzdání diplomové práce:*  06.05.2019

*Doba platnosti zadání je dva roky od data zadání.*

..........................................
*garant oboru*

..........................................
*vedoucí katedry*

..........................................
*děkan*

*V Praze dne*  22.10.2018

**Prohlášení:**

Prohlašuji, že jsem svoji diplomovou práci vypracoval samostatně a použil jsem pouze podklady ( literaturu, software, atd. ) uvedené v přiloženém seznamu.

Nemám závažný důvod proti užití tohoto školního díla ve smyslu § 60 Zákona č. 121/2000 Sb., o právu autorském, o právech souvisejících s právem autorským a o změně některých zákonů ( autorský zákon ).

V Praze dne 3.5.2019 Jan Půček

*Název práce:*

**Vliv nefaktorizovatelnosti svazku na stanovení luminozity v experimentu ALICE**

*Autor:* Jan Půček

*Obor:* Experimentální jaderná a částicová fyzika
*Druh práce:* Diplomová práce

*Vedoucí práce:* doc. Jesús Guillermo Contreras Nuňo, PhD., Katedra fyziky, Fakulta jaderná a fyzikálně inženýrská, České vysoké učení technické v Praze

*Abstrakt:*

Luminozita je na experimentu ALICE stanovena pomocí referenčního účinného průřezu změřeného ve van der Meer (vdM) skenech. VdM sken předpokládá faktorizovatelnost distribuce balíku do dvou nezávislých směrů. Pokud jsou směry korelované, luminozita je špatně stanovena pomocí vdM skenů a hodnota musí být opravena. V této práci byl vytvořen program simulující vdM skeny, který byl následně použit ke studiu efektů korelovaných balíků. Experimentální chyby jsou modelovány pomocí reálných dat. Program také testuje metodu používanou na experimentu ALICE pro různé modely balíků zahrnující korelaci. Je ukázáno, že vytvořený program v této práci je užitečný ke studiu stanovení luminozity na LHC.

*Klíčová slova:* Luminozita, ALICE, vdM kalibrace, Nefaktorizovatelnost

*Title:*

**Effect of beam non-factorisation**

**on luminosity determination in ALICE experiment**

*Author:* Jan Pŭček

*Supervisor:* doc. Jesús Guillermo Contreras Nuňo, PhD.

*Abstract:*

Luminosity is determined in ALICE using reference cross sections measured in van der Meer (vdM) scans. A vdM scan assumes factorisation of the bunch distribution into two independent directions. If the directions are correlated the luminosity determined by vdM scans is wrong and has to be corrected. In this thesis a program to simulate vdM scans was developed and used to study the effects of correlated bunches. The experimental uncertainties are modelled using real data. The program benchmarks the method used in ALICE for different bunch models which include correlations. It is shown that the program developed in this work is useful to study luminosity determination at the LHC.

*Key words:* Luminosity, ALICE, vdM calibration, Non-factorisation

## Acknowledgement

# Preface

Van der Meer scans are performed at the LHC to determined reference cross sections that are used later on to measure luminosity. The scans assume that the distribution describing the transverse profile of the colliding bunches, can be factorised in the two corresponding perpendicular directions. If these directions are correlated, the scan will yield wrong results that need to be corrected.

The method to estimate the correction and the uncertainty of this so called non-factorisation, assumes by necessity both a single Gaussian model of the luminosity region and a double Gaussian model for the bunch profiles.

In this thesis I have developed a suite of programs, based on the Monte Carlo method, to simulate vdM scans and test if the correction method at the LHC is appropriate when using single or double Gaussian models for the bunch profiles.

# Contents

# List of Figures

# Chapter 1

# Introduction

Determination of luminosity is a fairly forward process once everything works properly. The main difficulty is to correctly assign a measurement uncertainty and to apply corrections (for the case where not everything works as expected). Since there are several phenomena affecting the uncertainty (discussed in detail later), we have performed a systematic study on the determination of luminosity at the LHC, and focused in one of the less well known correction factors, which in occasions is one with the highest contribution to the measurement uncertainty. In short, this phenomenon is called transverse beam correlation. An illustration of this effect will be shown after discussing luminosity in Chapter 2 and describing a method of luminosity determination in Chapter 3. The goal of this thesis is to develop a program to simulate in detail van der Meer (vdM) scans as performed at the LHC and use the program to evaluate the method used in ALICE to correct for non-factorisation effects.

In order to ease the reading, several theoretical chapters are included, which may be skipped by an experienced reader. Chapter 2 introduces the physical quantity called luminosity. Several equations help to demonstrate different results for different collision conditions, which are useful later to formulate the luminosity determination at bunched colliders, see Chapter 3. In that chapter, there are also several common corrections applied to data obtained from vdM scans. The technical application of this method varies throughout different experiments. Since the work relates to data acquired by ALICE, Chapter 4 presents the experiment itself and also the realisation of the vdM scan. Chapter 5 begins the theoretical introduction to beam factorisation, which additionally includes the derivation of luminosity correction for beams with transverse correlation for the single Gaussian model of a bunch profile. The result of this derivation is crucial for benchmarking the numerical simulation we have created. Explanation and benchmarking results of the simulation can be found in Chapter 6. With this simulation we have created Monte Carlo data resembling the real acquired data. The MC data were then analysed with the same algorithm used for real data. This enabled us to compare the analysis output with the known input for different bunch models, which is discussed in Chapter 7.

Throughout the thesis, the Gaussian distribution will be often used. To keep the text uniform a standard integral is presented here in Eq. (1.1). The integral will be of use for computing luminosity and analytically computing the non-factorisation ratio in Chapter 5.

$$\int_{-\infty}^{\infty} \exp\left(-ax^2 - bx\right) = \sqrt{\frac{\pi}{a}} \exp\left(\frac{b^2}{4a}\right). \tag{1.1}$$

# Chapter 2

# Luminosity

Luminosity is a physical quantity, which relates the rate to the cross section of any process. Once the luminosity is determined for one process it can be used for other processes measured in the same set of collisions. This chapter will introduce several methods of luminosity determination with a deeper focus on the method of van der Meer (vdM) scans, which is further analysed in the next chapter. The theoretical calculations are needed for comparison with the simulation (more on this topic in Chapter 6), so one can cross check the numerical results.

The defining equation, where rate $R_P$, cross section $\sigma_P$ and luminosity $L$ are related, is Eq. (2.1).

$$R_P = L\sigma_P. \tag{2.1}$$

Luminosity is the proportional factor between rate and cross section. Furthermore one can derive Eq. (2.2), which involves two processes (A and B) and shows one of the first methods of measuring cross sections for different processes,

$$\sigma_B = \frac{R_B \sigma_A}{R_A}. \tag{2.2}$$

For colliders with bunched beams, it is possible to relate luminosity with the accelerator's parameters as shown in Eq. (2.3), where $K$ is a kinematic factor depending on the collision angle, $n_b$ is the number of bunches, $f$ is the revolution frequency, $N_{1,2}$ are the number of particles in the two colliding bunches and most importantly $S_{1,2}$ which are the bunch probability distributions.

$$L = K n_b f N_1 N_2 \int_{-\infty}^{\infty} S_1(x,y,z,t) S_2(x,y,z,t) \, \mathrm{d}x \, \mathrm{d}y \, \mathrm{d}z \, \mathrm{d}t. \tag{2.3}$$

This equation works only for head-on collisions. Other collision possibilities are collisions under a crossing angle or collisions with an offset. It is common to solve the integral under the assumption of Gaussian distribution functions, which is a fairly good description of the bunches' actual distribution (for the case of LHC bunches) and also it is possible to obtain analytical solutions. It has

to be stated, that the $z$ coordinate is coupled with time due to the movement of the bunches which in the Gaussian case is described as

$$\int_{-\infty}^{\infty} S_1(z + ct)S_2(z - ct)\,\mathrm{d}z\,\mathrm{d}t$$

$$= \left(\frac{1}{\sqrt{2\pi}\sigma_z}\right)^2 \int_{-\infty}^{\infty} \exp\left(-\frac{(z+ct)^2}{2\sigma_z^2}\right)\exp\left(-\frac{(z-ct)^2}{2\sigma_z^2}\right)\mathrm{d}z\,\mathrm{d}t$$

$$= \frac{1}{2\pi\sigma_z^2}\int_{-\infty}^{\infty}\exp\left(-\frac{(z^2 + 2zct + c^2t^2)+(z^2 - 2zct + c^2t^2)}{2\sigma_z^2}\right)\mathrm{d}z\,\mathrm{d}t$$

$$= \frac{1}{2\pi\sigma_z^2}\int_{-\infty}^{\infty}\exp\left(-\frac{(z^2 + c^2t^2)}{\sigma_z^2}\right)\mathrm{d}z\,\mathrm{d}t$$

where $\sigma_z$ is the bunch length or second moment of the Gaussian distribution. This can be separated and the result is shown in (2.4), which is the inverse value of the kinematic factor $K$ (for head-on collisions).

$$\int_{-\infty}^{\infty} S_1(z + ct)S_2(z - ct)\,\mathrm{d}z\,\mathrm{d}t = \frac{1}{2c}. \tag{2.4}$$

The previous part enables the treatment of the part depending on the transverse coordinates $x$ and $y$ to be performed independently (unless there is a correlation between the transverse and the longitudinal parts of the distribution). The following equations present the luminosity formulas for Gaussian bunches, which both have the same variance in each direction ($\sigma_x$, $\sigma_y$). For head-on collisions luminosity is computed by Eq. (2.5). A great property of the Gaussian distribution is that when collisions occur with an offset $\Delta x$, $\Delta y$, the offset can be factorised, which results into a product of head-on term with a coefficient as shown in Eq. (2.6).

$$L_{HeadOn} = \frac{n_b f N_1 N_2}{4\pi(\sigma_x\sigma_y)}, \tag{2.5}$$

$$L_{Offset} = L_{HeadOn}C_{Offset}, \quad C_{Offset} = \exp\left(-\frac{(\Delta x)^2}{4\sigma_x^2}\right)\exp\left(-\frac{(\Delta y)^2}{4\sigma_y^2}\right). \tag{2.6}$$

For collisions with crossing angle $\phi$ it will be assumed that $\phi$ is small and the angle denotes a tilt of the bunches in the $(x, z)$ plane. Under these assumptions it is possible to calculate the luminosity for collisions under a crossing angle, see Eq. (2.7).

$$L_{Angle} = L_{HeadOn}C_{Angle}, \qquad C_{Angle} = \frac{1}{\sqrt{1 + \left(\frac{\theta\sigma_z}{2\sigma_x}\right)^2}}. \tag{2.7}$$

Figure 2.1 shows a representative example of the correction factor for different angles. For an angle of 500 $\mu$rad the luminosity decreases by more than 10% for bunch dimensions close to those used at the LHC.
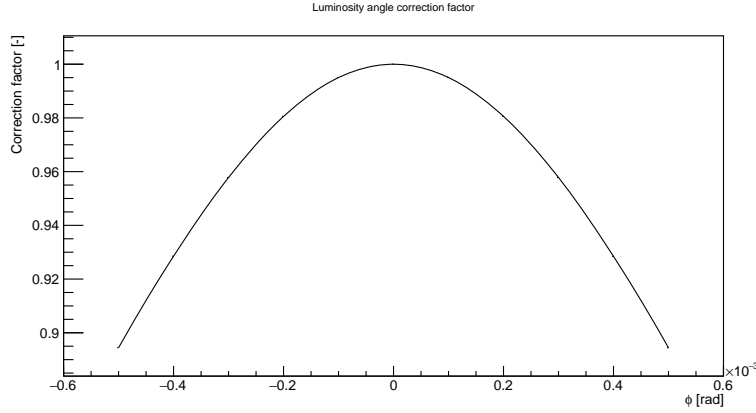
Figure 2.1: Angle correction factor for $\sigma_z = 5$ cm and $\sigma_x = 50$ $\mu$m.

Both phenomena (crossing angle, offset) decrease the luminosity, which is actually used in experiments like ALICE, which needs lower collision rate compared to ATLAS or CMS. However, the crossing angle is not used only to decrease the luminosity, but mainly to avoid collisions with satellites[1]. This type of collision is unwanted as they clog the detector and take place in unwanted locations.

A case, which is used rarely is beam offset while maintaining non-zero crossing angle. The equation to compute luminosity in this case is given in [1, p. 26]. The sketch of the situation is shown in Fig.2.2. Eq. (2.8) gives the non-trivial expression for luminosity under the conditions stated above.

$$L_{Off+Angle} = L_{HeadOn} C_{Offset} C_{CrossingAngle} \exp\left(\frac{B^2}{A}\right), \qquad (2.8)$$

$$A = \frac{\sin^2\Theta}{\sigma_y^2} + \frac{\cos^2\Theta}{\sigma_z^2}, \qquad B = \frac{\Delta y \sin\Theta}{2\sigma_y^2}, \qquad \Theta = \frac{\Phi}{2}.$$

A challenge nowadays is to enhance luminosity, while preserving the same crossing angle. A possible solution to this problem are crab waist and crab crossing collisions [4, 5] invented in the 1980's. The implementation at the LHC (SPS) was successful on 23 May 2018 and it will play a key role in the high luminosity upgrade [6].

The term luminosity has been introduced in this chapter and several theoretical cases of luminosity calculation have been presented. All presented equations

---

[1]The radio-frequency configuration of the LHC is such that the accelerator orbit is divided in 3564 slots of 25 ns each. Each slot is further divided in ten buckets of 2.5 ns each. In nominally filled slots, the particle bunch is captured in the central bucket of the slot. The charge circulating outside of the nominally filled slots is referred to as ghost charge; the charge circulating within a nominally filled slot but not captured in the central bucket is referred to as satellite charge.
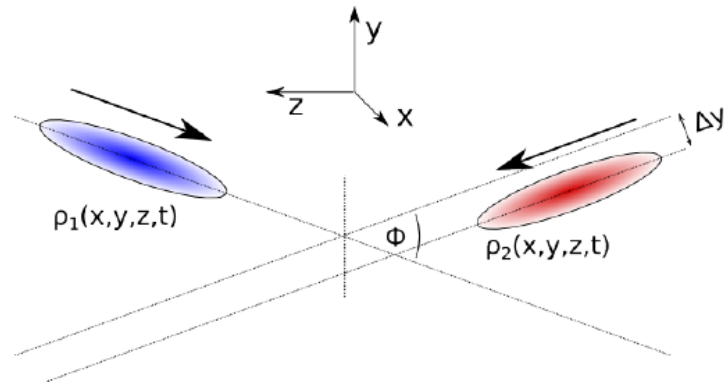
Figure 2.2: Sketch for the case where the bunches collide under the angle $\Phi$ and are shifted by $\Delta y$. Taken from [1].

will be of use in Chapter 6, where the uncertainties on the numerical simulation will be estimated. In my Bachelor thesis [7] one can find some of the analystical integrations needed in the intermediate steps leading to the equations presented in chapter.

# Chapter 3

# Van der Meer scan

The method [8] pioneered by Simon van der Meer in 1968 is most commonly used today at hadron colliders. Its aim is to calibrate a reference cross section for a corresponding detector, which is later used during data taking. The detector used as luminometer must be fast enough with short dead time. As a consequence the output of such a detector is only the rate of detected events. In order to relate this rate to an absolute value of luminosity a calibration is done.

This chapter will cover briefly the theory of this method and the next chapter will cover the experimental implementation at ALICE.

## 3.1 Theory

The van der Meer scan is based on the movement of beams in two orthogonal directions while measuring the rate of interactions. This enables us to specify a so called visible cross section $\sigma_{vis}$, which during data-taking plays the role of a reference cross section and the detectors used during the vdM scans act as luminometer measuring the rate of interactions. From Eq. (2.1) one determines the luminosity. To measure the visible cross section, it is needed to adapt Eq. (2.3). Because the process is independent of bunch distributions, it will remain in the form of $S_1(x, y, z)$ and $S_2(x, y, z)$. And as the movement is in two orthogonal directions, it will be assumed, that it is already integrated over $z$.

The luminosity for bunches with an offset of $(\Delta x, \Delta y)$, and *assuming* that $S_i(x, y) = S_i(x)S_i(y)$, equals

$$
L_{\text{VdM}}(\Delta x_0, \Delta y_0) = f n_b N_1 N_2
$$
$$
\int_{-\infty}^{\infty} S_{1x}(x) S_{2x}(x + \Delta x_0) \, \mathrm{d}x \int_{-\infty}^{\infty} S_{1y}(y) S_{2y}(y + \Delta y_0) \, \mathrm{d}y.
$$
(3.1)

As the beams will move in orthogonal directions separately, one can label the part integrating over $y$ as a constant (for one chosen separation $\Delta y$)

$$L_{\text{VdM}}(\Delta x, \Delta y_0) = C_y \int_{-\infty}^{\infty} S_{1x}(x) S_{2x}(x + \Delta x)\, \mathrm{d}x, \tag{3.2}$$

but the luminosity cannot be directly measured – Eq. (2.1) is used to switch luminosity for rate (a measurable quantity).

$$R(\Delta x, \Delta y_0) = \sigma_{vis} C_y \int_{-\infty}^{\infty} S_{1x}(x) S_{2x}(x + \Delta x)\, \mathrm{d}x, \tag{3.3}$$

$$\int_{-\infty}^{\infty} S_{2x}(x + \Delta x)\, \mathrm{d}\Delta x = \int_{-\infty}^{\infty} S_{2x}(x)\, \mathrm{d}x. \tag{3.4}$$

In Eq. (3.3) the visible cross section has been added. It is possible to integrate the equation in $\mathrm{d}\Delta x$ and use Eq. (3.4) to apply the normalisation of bunch distribution ($\int_{-\infty}^{\infty} S_i(x)\, \mathrm{d}x = 1$) to compute the integrated rate

$$\int_{-\infty}^{\infty} R(\Delta x, \Delta y_0)\, \mathrm{d}\Delta x = \sigma_{vis} C_y. \tag{3.5}$$

With this knowledge, it is possible to compute the integral in $x$ from Eq. (3.1) in the following manner

$$\int_{-\infty}^{\infty} S_{1x}(x) S_{2x}(x + \Delta x_0)\, \mathrm{d}x = \frac{R(\Delta x_0, \Delta y_0)}{\int_{-\infty}^{\infty} R(\Delta x, \Delta y_0)\, \mathrm{d}\Delta x}. \tag{3.6}$$

This means that once the rate of interactions is measured for different separations, the value of luminosity can be determined as

$$L_{\text{VdM}}(\Delta x_0, \Delta y_0) = f n_b N_1 N_2 \frac{R(\Delta x_0, \Delta y_0)}{\int_{-\infty}^{\infty} R(\Delta x, \Delta y_0)\, \mathrm{d}\Delta x} \frac{R(\Delta x_0, \Delta y_0)}{\int_{-\infty}^{\infty} R(\Delta x_0, \Delta y)\, \mathrm{d}\Delta y}. \tag{3.7}$$

In a simplified case the measured points are plotted into a graph, fitted by an appropriate function, which is integrated to obtain $\int_{-\infty}^{\infty} R(\Delta x_0, \Delta y)\, \mathrm{d}\Delta y$ or in the $x$-direction $\int_{-\infty}^{\infty} R(\Delta x, \Delta y_0)\, \mathrm{d}\Delta x$. An illustration of the possible scan outcome is in Fig.3.1.

In a real world scenario the scan outputs need to be corrected for several measurement artifacts (such as orbit drift, length-scale uncertainty, pileup etc.). In addition the measurement has to be corrected by the key assumption that the bunch distributions can be factorised into these two orthogonal directions (which is not always true). For these cases a generalisation of the vdM method has been developed which can be found in [9], where luminosity is computed as follows

$$L_{\text{VdM}}(\Delta x_0, \Delta y_0) = f n_b N_1 N_2 \frac{R(\Delta x_0, \Delta y_0)}{\int_{-\infty}^{\infty} R(\Delta x, \Delta y)\, \mathrm{d}\Delta x\, \mathrm{d}\Delta y}. \tag{3.8}$$

The great disadvantage of this approach is the high time demand. For this reason it is not used at LHC.
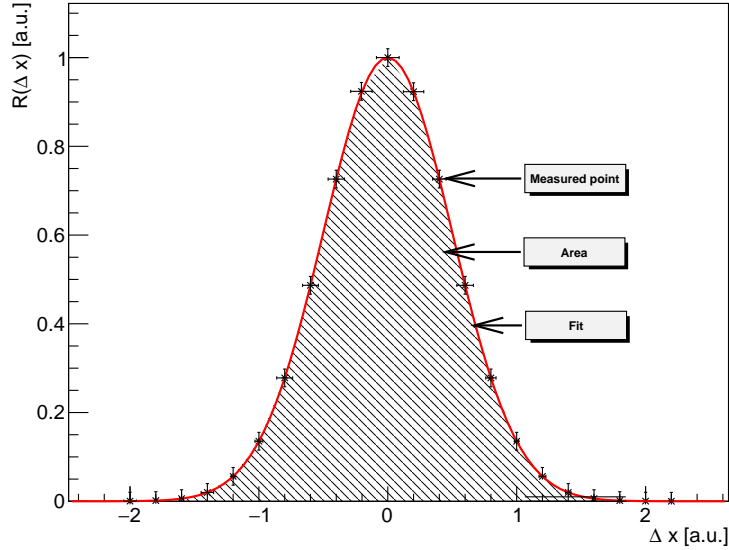
Figure 3.1: Rate of interaction measured at each $\Delta x$-separation represented by a black point, which are fitted by a red function (here Gaussian). The fit is integrated to obtain the area under the curve which is equal to the integrated rate needed in determination of the luminosity using Eq. (3.7).

## 3.2 Corrections

In this section several corrections to the vdM scan data will be discussed: correction to the length of the step, correction for the orbit drift and $XY$-correlations.

First of all, the calibration is done separately for each bunch pair as the bunch population may change. The results are later combined, however, for the analysis they are treated separately.

During the vdM scan a length-scale calibration is performed, which "calibrates" the beam offset. The goal of this correction is to fine tune the conversion factor between magnet current and the beam displacement. That is why both beams are shifted in the same direction and the centre of the luminosity region is measured by the trackers in the experiments. The measured shift is compared with the machine input. A linear fit determines the correction needed. For example in 2015 at CMS the correction factor was 0.983 (0.985) in the horizontal (vertical) direction [10].

The orbit drift is a more complex problem. It has different effects in the scan plane and in the non-scan (constant) plane. The drift narrows or widens the scan curve in the scan direction, depending on the direction of drift and assuming

constant velocity of the drift. In the non-scan plane the effect is different − the
scan behaves as if the axis are tilted (not orthogonal) − see Fig.3.2.
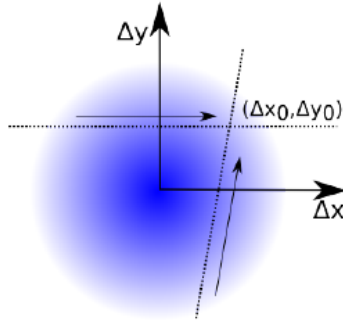


Figure 3.2: Deformation of axis during vdM scan with constant drift velocity.
Taken from [1].


As described earlier, in general one cannot assume factorisable bunches. The
effect of non-factorisation has been studied in [7], where it is estimated, that
the correction can be as high as 3% − depending on the correlation factor in
the bunches. To measure the correction, primary vertices are reconstructed and
fitted by appropriate bunch distributions − different for each bunch crossing.
Then the correction factor is extracted from the fit parameters. More on this
topic can be found in Chapter 6.

This chapter has given a brief overview of the van der Meer scan method.
With the main focus of this work on the LHC, more information about imple-
menting this method will be presented in the next chapter.

# Chapter 4

# Luminosity determination in ALICE

There are four main experiments at the LHC, each having a different research goal. Due to the focus on different aspects of particle collisions the detectors and methods of obtaining data vary. However, all four experiments use the vdM scan to calibrate absolute luminosity. The difference is in the experimental setup and application of corrections. The best precision of the luminosity measurement on a bunched hadron collider is 1.16% determined by LHCb (year 2014, [11]). Due to working with the ALICE collaboration, this chapter will focus only on describing ALICE and its methods of obtaining luminosity.

One common measurement is done for every experiment at the LHC and that is bunch population measurement, which appears in Eq. (2.3) under the $N_{1,2}$. To measure the bunch population several special devices have been developed at the LHC. A DC current transformer (DCCT), a device based on the flux-gate magnetometer principle, measures the total beam population – meaning it cannot distinguish between bunches. Its resolution and range are astonishing having $1\mu$A as rms for 1s average and a range from $8\mu$A to 860mA. To measure the bunch-by-bunch population a Fast Beam Current Transformer is used. It cannot measure absolute values of bunch population, but only relative. However, it is capable of measuring all 3564 nominal bunches scaled to 25ns slots. In order to assign absolute values, the sum of all fractions are scaled to the value obtained by the DCCT. At the LHC there are two DCCTs and two FBCT per beampipe [12, 13].

## 4.1   ALICE

A Large Ion Collider Experiment (ALICE) is optimised for heavy ion collisions, which means that the 19 sub-detectors have to track and identify the tens of thousands of particles produced in each collision. The research goal of this experiment is to study matter heated to 10000 times the temperature of the Sun and to answer why protons and neutrons weight more than 100 times more than the quarks they are made of [14]. An overview of the whole experiment with labels of all subsystems is shown in Fig.4.1.



THE ALICE DETECTOR

a. ITS SPD (Pixel)
b. ITS SDD (Drift)
c. ITS SSD (Strip)
d. V0 and T0
e. FMD

1. ITS
2. FMD, T0, V0
3. TPC
4. TRD
5. TOF
6. HMPID
7. EMCal
8. DCal
9. PHOS, CPV
10. L3 Magnet
11. Absorber
12. Muon Tracker
13. Muon Wall
14. Muon Trigger
15. Dipole Magnet
16. PMD
17. AD
18. ZDC
19. ACORDE
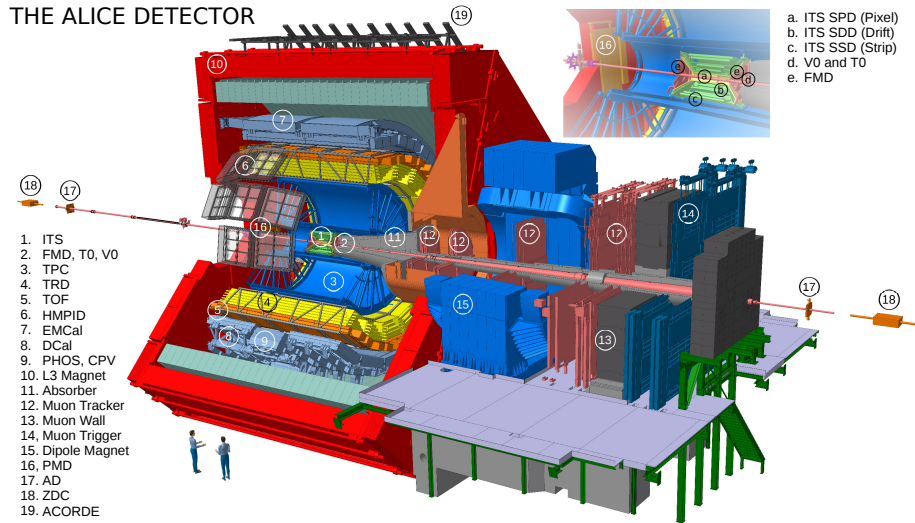
Figure 4.1: The ALICE in a 3D computer model, taken from [2].

Closest to the beampipe is the Inner Tracking System consisting of mainly semiconductor detectors. Surrounding it is the Time Projection Chamber, capable of tracking particles over large distances while obtaining all three spatial components. Since the experiment is encapsulated by a magnet which steers charged particles, it is possible to compute momentum of the particles passing through the detector system.

ALICE uses two detectors, which serve as luminometers. Both detectors have two parts which are located at both sides of the interaction point. The V0 has parts A and C, each consists of 32 scintillator tiles. V0-A is 340 cm from the nominal interaction point (IP) and V0-C is 90 cm from the IP along the beam axis. The detector T0 has as well parts A and C, each being an array of 12 Cherenkov counters. T0-A is 370 cm from the IP and T0-C is 70 cm from the IP (one is behind the V0-A and the second is in front of the V0-C). Both V0 and T0 have great time resolution and thus serve as triggers for the other
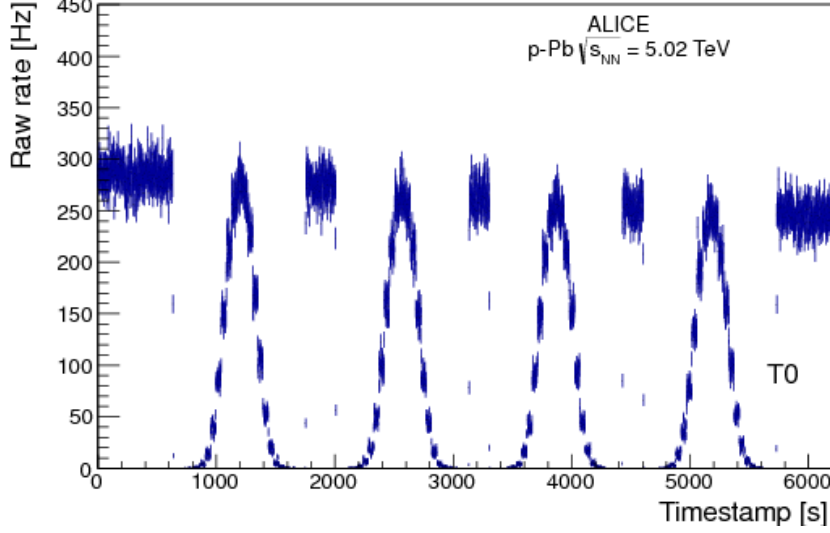
Figure 4.2: Raw rate measured by T0 detector during vdM scan in 2014 proton-lead collisions. Taken from [3]

sub-detectors. They provide information about $z$-position of the primary vertex (T0) and rate of interaction (T0 and V0).

The methodology that has been used during the 2013 p-Pb (Pb-p) vdM scan will be presented. Due to the asymmetric setup of luminometers and the shift of the centre-of-mass frame, the vdM scan had to be done for both configurations. The boundaries for beam movement have been set as $\pm 6\sigma_b$ (6 expected bunch widths). The vdM scan consists of 2 repeated scans, each including a X and a Y scan. The first scan was made in the horizontal direction and then in the vertical, while shifting the beam from negative to positive. The second scan was the same as the first one except the shifting, which was done from positive to negative. The scan in each direction was measured at 25 points, where every point was measured for 30 seconds [3]. Also during the scan, the number of bunches is reduced to be able to measure collisions of bunch with residual gas molecules or ghosts/satellites. All this information is needed in order to create a simulation with conditions similar to real life.

### 4.1.1 Vertex reconstruction

The primary vertex is the precise position where a collision took place. This collision generates primary particles. The particles leave a signal inside the detectors, which can be reconstructed into positions. All positions of a single particle make up its trajectory in the detector. In case of ALICE, these detectors are ITS and TPC as presented earlier. However, during a collision there may be up to several thousands particles, making it difficult to distinguish them. There are several possible approaches to reconstruct tracks: starting from the points closest to the collision or from the other end by reconstructing tracks from the most outside positions. But this section does not focus on track reconstruction, its main focus is on the vertex finding and vertex fitting algorithms.

The vertex finding algorithm selects tracks, which have the same primary vertex. This is done by extrapolating the track to their origin and grouping tracks within a certain range of distance among themselves. To be able to reconstruct a vertex at least 5 tracks are needed. The more tracks point toward the same spot the better. However, in high multiplicity events some of the tracks might be fake. This means that the vertex finding is always a compromise. The goal of the vertex fitting algorithm is to obtain the best fit coordinates of the vertex. The precise method used at ALICE is described in [15]. In short the algorithm minimises a $\chi^2$ function, which is a sum over all tracks, "weighted" by the precision of the track. The output is the vertex position (with $x$, $y$ and $z$ coordinates) and covariance matrix of a 3D Gaussian distribution which accounts for the measurement uncertainty.

### 4.1.2 Non-factorisation determination in ALICE

The primary vertices are used for measurement of the so called luminosity region, which is an input for the non-factorisation analysis. Since the real bunch distributions are not known, there are several assumptions made with respect to the technique used for analysis. First, in order to use analytically the covariance matrix of the measured primary vertices, we compute the mean, variance and correlation of the luminosity region for each set of primary vetrices obtained in each vdM scan step under the assumption of single Gaussian bunch profiles. Then, in order to estimate non-factorisation, we assume double Gaussian bunch profiles and the parameters are fitted to correspond to measured means, variances and correlations of luminosity regions. The double Gaussian model is assumed because it allows to compute analytically the luminosity including corrrelations and as determined in the vdM scans. The ratio of these two luminosities is the non-factorisation correction. To assign an uncertainty to this method, the fit parameters are varied within their fit uncertainties and the non-factorisation ratio is recomputed. The maximum/minimum from 50 variations is taken as 1 sigma uncertainty. To understand the assumptions and their effects on the analysis, the procedure has to be checked with simulations.

### 4.1.3   Offset and diagonal scans

Offset scans have working points different to (0;0), meaning the collisions are not head-on at the common point in both directions of the vdM scan. The advantage is obtaining more scan points, which improves the precision of vertex fitting plus serves as cross-check of data that has been already taken. The downside is higher sensitivity to systematic effects [11].

In 2018, for the PbPb vdM scan, an additional scan has been added in the diagonal directions. First both beams were moved apart by $2.5\sigma$ from head-on position on the $y = x$ axis. Then they cross over in 20 steps, so the final configuration is the same as initial, just with swapped beams. Data taking at each step takes 30 seconds. Second scan is similar, only the beams move on the axis where $y = -x$. This diagonal scan should enable determination of the beam non-factorisation with higher precision, where the greatest advantage will probably be for the method using primary vertices.

# Chapter 5

# Beam factorisation

The assumption of bunch shape factorisation may not hold true during van der Meer scans. There are models which enable us to study this effect analytically, which will be shown in this chapter. In order to describe the most important parts, only the simplest model (single Gaussian in 2D) will be used in the following calculations. The goal of this demonstration is to compute the ratio of the luminosity without assumption of factorisation (will be further called true) and the luminosity obtained by measuring the rate while moving the beams separately in two orthogonal directions (by the vdM method, will be further called vdM).

The 2D single Gaussian distribution in Eq. (5.1) includes a correlation factor $\rho$, when the factor is non-zero the distribution cannot be factorised. To shorten the derivation of the true luminosity Eq. (5.2) from [16] will be used.

$$G(x,y) = \exp\left[-\frac{1}{2(1-\rho^2)}\left(\frac{(x-\mu_x)^2}{\sigma_x^2} + \frac{(y-\mu_y)^2}{\sigma_y^2} - \frac{2\rho\,(x-\mu_x)\,(y-\mu_y)}{\sigma_x\sigma_y}\right)\right].$$
(5.1)

$$L_{\text{true}*} = \frac{\sqrt{|\mathbf{K}|}}{2\pi\sqrt{|\sigma_\mathbf{a}||\sigma_\mathbf{b}|}}.$$
(5.2)

$$\sigma_\mathbf{a} = \begin{pmatrix} \sigma_{x1}^2 & \rho_1\sigma_{x1}\sigma_{y1} \\ \rho_1\sigma_{x1}\sigma_{y1} & \sigma_{y1}^2 \end{pmatrix},$$

$$\sigma_\mathbf{b} = \begin{pmatrix} \sigma_{x2}^2 & \rho_2\sigma_{x2}\sigma_{y2} \\ \rho_2\sigma_{x2}\sigma_{y2} & \sigma_{y2}^2 \end{pmatrix},$$

$$\mathbf{K}^{-1} = \sigma_\mathbf{a}^{-1} + \sigma_\mathbf{b}^{-1}.$$

Please note that $\mathbf{K}$ has this simple form only for head-on collisions. The $\sigma_a$ is the covariance matrix of the first bunch and $\sigma_b$ is the covariance matrix of the second bunch. Since only the determinant of $\mathbf{K}$ is needed, it is possible to

use the equivalence between the inverse value of matrix determinant with the determinant of inverse matrix

$$\det(K) = \frac{1}{\det(K^{-1})}.$$

The result is then described in Eq. (5.3). It is visible, that the expression is symmetrical to the change of bunch labeling (changing 1 by 2). This is the expected behavior since they both are described by the same model. Same behavior is expected for the second part of computation – vdM luminosity, where a different approach is used.

$$L_{\text{true}*} = \frac{1}{2\pi\sqrt{\sigma_{x1}^2\sigma_{y1}^2(1-\rho_1^2) + \sigma_{x2}^2\sigma_{y2}^2(1-\rho_2^2) + \sigma_{x1}^2\sigma_{y2}^2 + \sigma_{x2}^2\sigma_{y1}^2 - 2\sigma_{x1}\sigma_{y1}\sigma_{x2}\sigma_{y2}\rho_1\rho_2}}.$$
$$(5.3)$$

To calculate the luminosity for each separation a triple integral will be used. First integration will eliminate the dependence on the beam separation. And then it is possible to integrate over $x$ and $y$. To simplify the algebraic process, a substitution was made, see Eq. (5.4). The computation alone is afterwards straight forward using the standard integral Eq. (1.1). The result is shown in Eq. (5.5).

$$A = \frac{1}{4\pi\sigma_{x1}\sigma_{y1}\sigma_{x2}\sigma_{y2}\sqrt{1-\rho_1^2}\sqrt{1-\rho_2^2}},$$
$$a_1 = \frac{1}{2(1-\rho_1^2)\sigma_{x1}^2},$$
$$a_2 = \frac{1}{2(1-\rho_2^2)\sigma_{x2}^2},$$
$$a = a_1 + a_2,$$
$$b = \frac{1}{2(1-\rho_1^2)\sigma_{y1}^2} + \frac{1}{2(1-\rho_2^2)\sigma_{y2}^2},$$
$$c_1 = \frac{\rho_1}{(1-\rho_1^2)\sigma_{x1}\sigma_{y1}},$$
$$c_2 = \frac{\rho_2}{(1-\rho_2^2)\sigma_{x2}\sigma_{y2}},$$
$$c = c_1 + c_2. \qquad\qquad (5.4)$$

$$G_1 G_2(\Delta x, 0) = A \exp\left[-x^2 a - 2x\Delta x a_1 - \Delta x^2 a_1 - y^2 b + xyc + \Delta xy c_1\right].$$

$$\int G_1 G_2(\Delta x, 0)\,\mathrm{d}\Delta x = A\sqrt{\frac{\pi}{a_1}}\exp\left[-x^2 a_2 + xyc_2 - y^2\left(b - \frac{c_1^2}{4a_1}\right)\right].$$

$$\int\int G_1 G_2(\Delta x, 0)\,\mathrm{d}\Delta x\,\mathrm{d}x = A\sqrt{\frac{\pi}{a_1}}\sqrt{\frac{\pi}{a_2}}\exp\left[-y^2\left(b - \frac{c_1^2}{4a_1} - \frac{c_2^2}{4a_2}\right)\right].$$

$$\int\int\int G_1 G_2(\Delta x, 0)\,\mathrm{d}\Delta x\,\mathrm{d}x\,\mathrm{d}y = A\frac{\pi}{\sqrt{a_1 a_2}}\sqrt{\frac{\pi}{b - \frac{c_1^2}{4a_1} - \frac{c_2^2}{4a_2}}},$$

$$\int\int\int G_1 G_2(\Delta x, 0)\,\mathrm{d}\Delta x\,\mathrm{d}x\,\mathrm{d}y = \frac{1}{\sqrt{2\pi(\sigma_{y1}^2 + \sigma_{y2}^2)}}.$$

$$L_{\mathrm{VdM}*}(0,0) = \frac{R(0,0)}{\int_{-\infty}^{\infty} R(\Delta x, \Delta y_0)\,\mathrm{d}\Delta x}\frac{R(0,0)}{\int_{-\infty}^{\infty} R(\Delta x_0, \Delta y)\,\mathrm{d}\Delta y}.$$

$$L_{vdM*} = 2\pi\sqrt{(\sigma_{x1}^2 + \sigma_{x2}^2)(\sigma_{y1}^2 + \sigma_{y2}^2)}L_{true*}^2. \qquad (5.5)$$

Once both expressions (true luminosity and vdM luminosity) are divided, the non-factorisation ratio is obtained, Eq. (5.6). When both correlation factors $\rho_{1,2}$ are zero, the ratio is equal to one. The ratio can be equal to one even in cases when Eq. (5.7) is satisfied – bunches alone exhibit non-factorisation, but their product does not. It may seem that non-factorisation is only disadvantageous, however, from purely mathematical point of view, it can enhance luminosity once the sign of correlation factors is the same (a detailed study, prediction and a recommendation of skew quadrupole usage is far beyond the scope of this work).

$$R = \sqrt{1 - \frac{\sigma_{x1}^2\sigma_{y1}^2\rho_1^2 + \sigma_{x2}^2\sigma_{y2}^2\rho_2^2 + 2\sigma_{x1}\sigma_{y1}\sigma_{x2}\sigma_{y2}\rho_1\rho_2}{\left(\sigma_{x1}^2 + \sigma_{x2}^2\right)\left(\sigma_{y1}^2 + \sigma_{y2}^2\right)}}, \qquad (5.6)$$

$$\rho_1 = -\frac{\sigma_{x2}\sigma_{y2}}{\sigma_{x1}\sigma_{y1}}\rho_2. \qquad (5.7)$$

If the experiment would only acquire rates of interaction at different separations, one would never be able to tell the parameters needed for this kind of analysis. This is the reason why experiments complement measuring rates with primary vertex reconstruction as described earlier, which enables indirect measurement of non-factorisation. In order to verify this approach a simulation has been created.

# Chapter 6

# Scan simulation

The simulation is coded in C++ within the ROOT framework [17]. The idea of the simulation is first to generate random points in three dimensions following a given bunch distribution and fill them into a histogram. The histogram represents a bunch, which is later overlapped with another bunch (this corresponds to the integral over time) to create a luminosity region. The luminosity region is integrated to obtain the luminosity value for that particular collision. In a later phase of the analysis the points in the luminosity region will be smeared using the uncertainty covariance matrices obtained by ALICE from their measurement of the primary vertex.

As a first step, each part of the simulation has to be verified, at least for simple bunch distributions – cases that can be compared to an analytical computation. This benchmarking to evaluate the analysis code will be further detailed in the next chapter.

The whole simulation code consists of several classes, each with a different purpose. Figure 6.1 is a schematic sketch of the algorithm with key functions written over the arrows. The class vdM_Bunch serves as initial stepping stone into the simulation. In this class all distribution parameters are set and random points are generated. Points from two vdM_Bunch classes are input into vdM_Interaction class which enables setting many collision parameters (shift, crossing angle, step sizes etc.). By calling the function collide, one obtains the luminosity value for the selected collision and may also obtain the vertex distribution of the luminous region. This part of the text will deal with luminosity values only.

## 6.1 Benchmarking

The goal of benchmarking is to check all parts of the simulation for potential programming errors by looking for the behaviour which would differ from analytical expectations. The generation of bunches has been verified in my Bachelor thesis [7, p. 41-46]. One remark to be made concerning the widths of 1D cuts
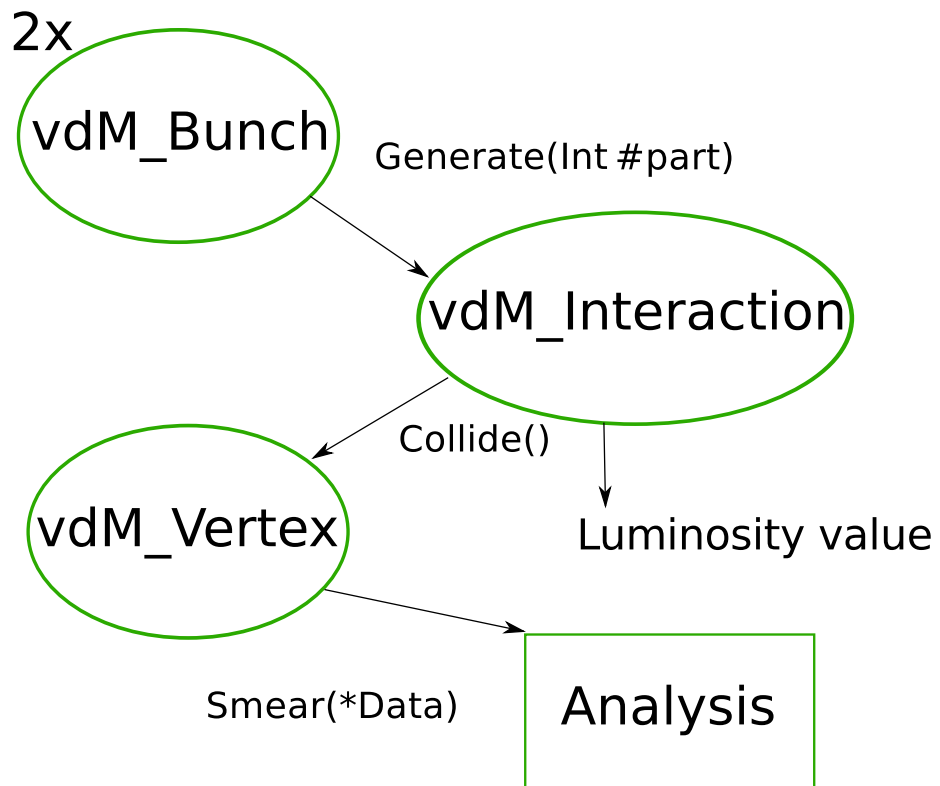
Figure 6.1: Scheme of collision simulation.

made to 2D distribution − in my B. Sc. thesis was a bias of 2-4%. This was later resolved − the histogram bins contained low number of entries, which in turn meant lower $\sigma$ when fitted by the $\chi^2$ method. Once the likelihood method was used all values were equal to the analytical ones.

Several phenomena were controlled and compared to analytical predictions − luminosity in head-on collisions, effect of a crossing angle $(y - z)$, the bunch width determined by a simulated vdM scan and the effect of non-factorisation (more in Sec. 6.3).

Histograms consist of discrete bins which are filled with entries. This means that Eq. (2.3) cannot be used with the integral. Instead a sum is used − to get the total number of entries summing the complete histogram over all bins − see Eq. (6.1), where $n$ is the total number of entries and the distribution is assumed to be normalised. The difference is in the computation of the luminosity region. To get a luminosity region two bunches are overlapped, both histograms having the same bin widths in each direction. But to normalise this procedure one has to divide by the bin-widths $\Delta x$, $\Delta y$. The reason one does not need to account for $\Delta z$ is that it is already summed. To obtain a luminosity value from the luminosity region it is sufficient to multiply by the kinematic factor as shown in Eq. (6.2) − the $n_b$ (number of bunches) and $f$ (frequency) are set to 1 and are not shown anymore, because they will cancel in the ratio of luminosities.

$$n \int_{-\infty}^{\infty} S_i(x, y, z) \, \mathrm{d}x \, \mathrm{d}y \, \mathrm{d}z = \sum_{x,y,z=0}^{Nbins} H_i(x, y, z). \tag{6.1}$$

$$KN_1N_2 \int_{-\infty}^{\infty} S_1(x, y, z + ct) S_2(x, y, z - ct) \, \mathrm{d}x \, \mathrm{d}y \, \mathrm{d}z \, \mathrm{d}t =$$
$$\sum_{x,y,z=0}^{Nbins} \sum_{i=-Nbinsz}^{Nbinsz} \frac{H_1(x, y, z + i) H_2(x, y, z - i)}{\Delta x \Delta y}. \tag{6.2}$$

To be able to compare the simulation (right side of Eq. 6.2) one must compute the left side, which is already done for head-on collisions with single Gaussian bunch distributions shown in Eq. (2.5). A graph has been made to compare the analytical prediction with the output of the simulation see Fig.6.2. There seems to be a systematic offset of 0.3% and an RMS of 0.3%. It is worth noting that the point of (0.55, 0.55) is very far away from unity and is suspected to have a rounding/overflow issue. In all the following text we will be using a generous uncertainty of 0.5% arising from the random generation.

To verify the correct behaviour of the simulation during collisions with crossing angle, Eq. (2.7) was used. The dependence of the luminosity on the crossing angle was plotted. A fit was done to estimate the simulation uncertainty − the only variable parameter was $p1$ which is shown in Eq. (6.3). The other parameter which is fixed is the $p0$ which only represents the fraction $\frac{\sigma_z}{2\sigma_x}$. The uncertainty on $p1$ is 1% and it is clearly overestimated. This was achieved by
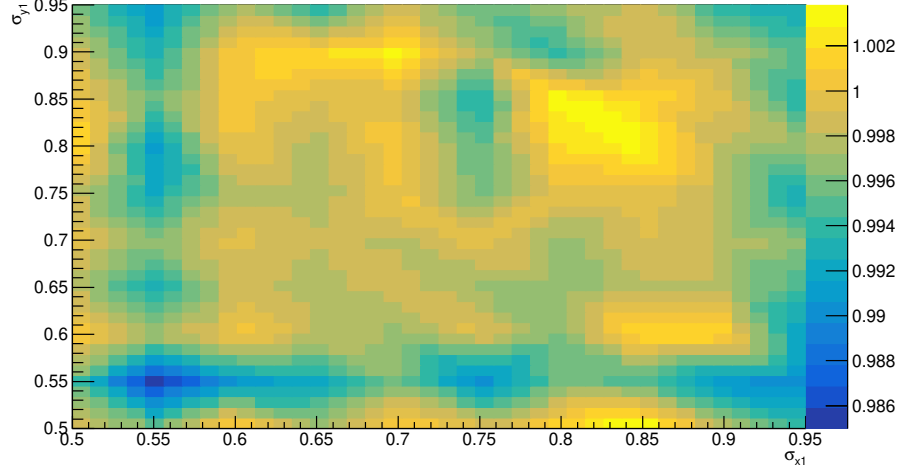
Figure 6.2: Comparison of computed luminosity to analytically predicted luminosity (their ratio on palette), dependent on the bunch widths in $x$ (on $x$-axis) and $y$ (on $y$-axis).

using the computed value of head-on luminosity instead of the analytical value, which on its own has a 0.5% uncertainty. The result is shown in Fig. 6.3.

$$\frac{L_{Angle}}{L_{HeadOn}} = \frac{1}{\sqrt{1 + p1 \left(\frac{\theta \sigma_z}{2\sigma_x}\right)^2}}. \tag{6.3}$$

Other two checks need to be made, before computing the uncertainties for more complicated cases. One is a vdM scan, which should obey the offset given by Eq. (2.6). To make understanding easier, the ratio of the offset luminosity to the head-on luminosity was plotted and fitted by a Gaussian function. The width of the fit $\sigma_f$ was expected to be $\sqrt{2}\sigma_{x,y}$ depending on the direction of the offset. For the parameters used in the simulation the expected width was $\sigma_{f-ex} = 0.07071$ and the one obtained from the simulation was $\sigma_f = (0.07066 \pm 0.00003)$. The generated data and fit is in Fig.6.4.

The last verification involves a vdM scan with a crossing angle, because the dependence is more complex, than a multiplication of two correction factors – as was already shown in Eq. (2.8). The correction factor can be rearranged to get Eq. (6.4). For a well visible effect, the common simulation values had to be adjusted – $\sigma_y = 0.05$, $\sigma_z = 5.2$ and the crossing angle $\Theta = 0.01$. The vdM scan should output a Gaussian function with width $\sigma_{ex} = 0.102021$. The result of the simulation is in Fig. 6.5, which reveals the fit value being $\sigma_f = (0.10238 \pm 0.00009)$.
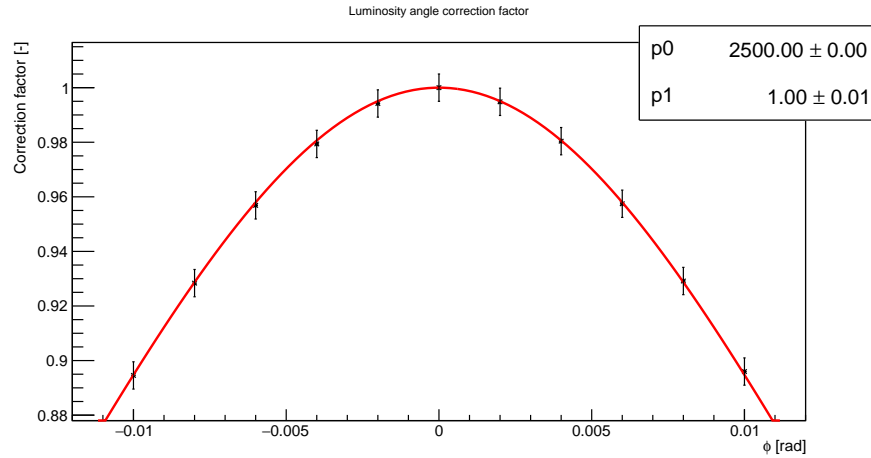
Figure 6.3: Dependence of luminosity on collision angle. The bunch parameters were: $\sigma_{x,y} = 0.1$, $\sigma_z = 5.0$ – both bunches had the same widths. The simulation corresponds to the analytical model with an uncertainty better than 1%.
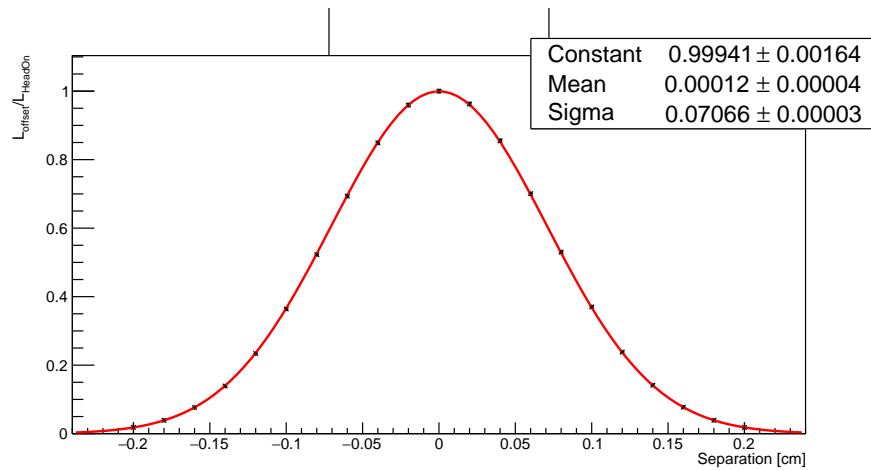


Figure 6.4: Simulated vdM scan to verify the analytically predicted behaviour.

$$C = \exp\left[-\frac{\Delta y^2}{4\sigma_y^2}\left(1 - \frac{\sigma_z^2\sin^2\Theta}{\sigma_z^2\sin^2\Theta + \sigma_y^2\cos^2\Theta}\right)\right]. \tag{6.4}$$

Overall these simple cases of single Gaussian have very precise results and once luminosity ratios of generated values are used it is possible to obtain uncertainty of tenths of percent.
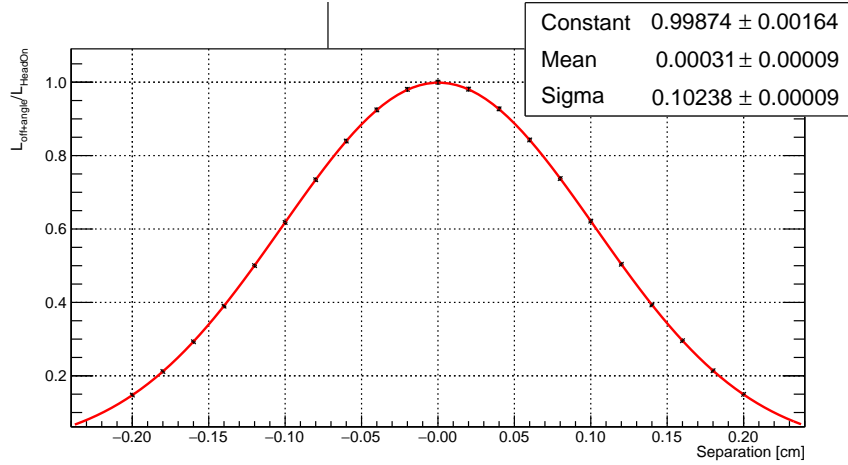


Figure 6.5: Simulation output showing the results for the vdM scan in the $y$-direction while maintaining the crossing angle. This is the last benchmark using single Gaussian bunch profiles to obtain the simulation uncertainty.

## 6.2    Simulation uncertainties

In this section, first the general formula for head-on collisions of Gaussian bunches will be given, which will be useful to evaluate the simulation using double Gaussian bunch profiles. From the benchmarking the uncertainties for a single Gaussian are known. Thus it is possible to estimate the uncertainties for double Gaussian bunches and compare the prediction with the results of a simulation. This will be important for studies presented later in this work to accurately simulate the difference of luminosity determined by a vdM scan and by the simulation.

The most general formula for a head-on luminosity for two colliding Gaussian bunches is in Eq. (6.5) – bunch "1" has widths $\sigma_{1x,y}$, bunch two is defined by widths $\sigma_{2x,y}$. To understand the usefulness in the case of a double Gaussian bunch profile collisions, it is needed to present the double Gaussian distribution

beforehand.

$$L_{\text{HeadOn}} = \frac{n_b f n_1 n_2}{2\pi\sqrt{(\sigma_{1x}^2 + \sigma_{2x}^2)(\sigma_{1y}^2 + \sigma_{2y}^2)}}. \tag{6.5}$$

The double Gaussian distribution is a sum of two single Gaussian distributions with a condition − both single Gaussians have the same mean. In order to leave the distributions normalised the weight factor $w$ is added as shown in Eq. (6.6), where $G$ represents a single Gaussian.

$$DG = wG_A + (1 - w)G_B. \tag{6.6}$$

Now to compute the head-on luminosity, the equation will reduce to four parts, each consisting of a single Gaussian part. This way Eq. (6.5) is used. To make it clear a schematic Eq. (6.7) demonstrates the collision of bunch 1 (consists of Gaussians A and B) with bunch 2 (consists of Gaussians C and D). We want to obtain an estimate of the simulation uncertainty, each integral has a relative error $\sigma_{rel}$ determined in Sec. 6.1 − $\sigma_{rel} = 0.5\%$. This value is used for every integral in Eq. (6.7) and all uncertainties were summed in quadrature. This fact is expressed in Eq. (6.8), where integrals are noted by subscripts of constituents from Eq. (6.7).

$$L = Kn_1 n_2 \int_{-\infty}^{\infty} \left(W_1 G_{1A} G_{2C} + W_2 G_{1A} G_{2D} + W_3 G_{1B} G_{2C} + W_4 G_{1B} G_{2D}\right) \mathrm{d}V\,\mathrm{d}t. \tag{6.7}$$

$$\sigma_L = \sigma_{rel}\sqrt{K_1 + K_2 + K_3 + K_4}, \tag{6.8}$$
$$K_1 = (w_1 w_2 1A2C)^2,$$
$$K_2 = (w_1(1 - w_2)1A2D)^2,$$
$$K_3 = ((1 - w_1)w_2 1B2C)^2,$$
$$K_4 = ((1 - w_1)(1 - w_2)1B2D)^2.$$

The following values are used for the simulation: $\sigma_{1B-x,y} = 0.5$[1], $\sigma_{2C-x,y} = 0.3$, $\sigma_{2D-x,y} = 0.5$, $\sigma_{z-1A,2C} = 6.0$, $\sigma_{z-1B,2D} = 5.0$, $\Theta = 0$ and $w_{1,2} = 0.5$. The other parameters were varied in the range from 0.2 to 0.7 separately by steps of 0.05. From this knowledge the relative uncertainty calculated by Eq. (6.8) is around 0.25%. The output is in Fig.6.6, where for the most part the ratio is less than 0.27% away from unity determined from Fig.6.7.

---

[1]The main interest is to model a real life case, which can be done by choosing proportional values of bunch widths. This is the reason of omitting units in the text. The only need of assigning units is for vertex distribution, which must correspond to real-life covariance matrix element units.
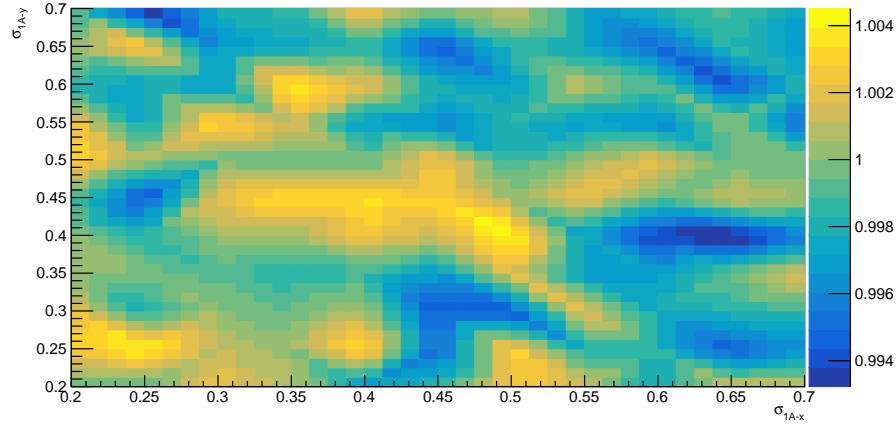
Figure 6.6: Benchmarking simulation for Double Gaussian bunch profiles. The $z$-axis/palette represents the ratio of the simulated luminosity divided by the analytically predicted luminosity.
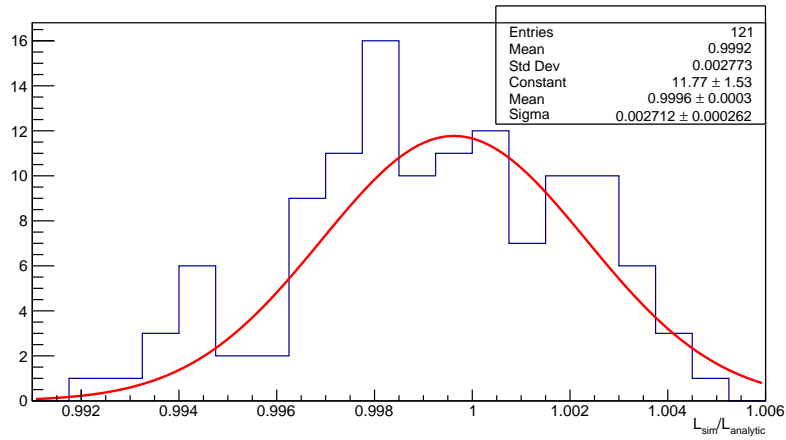


Figure 6.7: Histogram created from the $z$-values of Fig.6.6. Values are fitted by a Gaussian function to obtain the uncertainty of the simulation.

## 6.3 Bunch non-factorisation

So far we have verified the components of the simulation, the creation of random points, the overlap under different conditions. And we have set an upper uncertainty bound to this approach. It is also needed to compare whether the analytically computed non-factorisation ratio is equal to the ratio obtained by the pure simulation (computing both true and vdM luminosity via numerical simulation).

First, only simulating head-on luminosity was tested while varying the correlation factor of one of the beams while keeping the other correlation constant. This scenario was already presented analytically for the single Gaussian model in Chapter 5. The result is plotted in Fig. 6.8. The important result here is the luminosity enhancement for the correlation factor of the first beam is not equal to minus the correlation factor of the second beam ($\rho_1 \neq \rho_2$). The red curve is expressed in Eq. (6.9).

$$L_{\text{true}*} =$$

$$\frac{1}{2\pi\sqrt{\sigma_{x1}^2\sigma_{y1}^2(1-\rho_1^2) + \sigma_{x2}^2\sigma_{y2}^2(1-\rho_2^2) + \sigma_{x1}^2\sigma_{y2}^2 + \sigma_{x2}^2\sigma_{y1}^2 - 2\sigma_{x1}\sigma_{y1}\sigma_{x2}\sigma_{y2}\rho_1\rho_2}}.$$
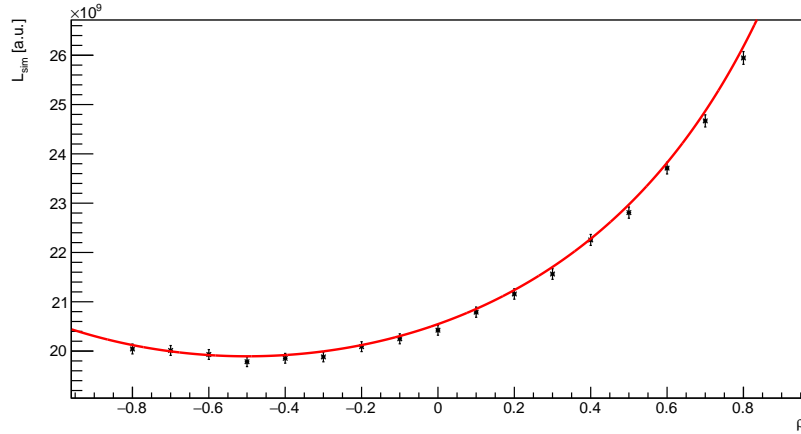
$$(6.9)$$



Figure 6.8: Dependence of luminosity on correlation factor $\rho$. The parameters used for the simulation: $\sigma_{x1} = \sigma_{x2} = \sigma_{y1} = \sigma_{y2} = 0.2$, $\rho_1 = \rho$, $\rho_2 = 0.5$. Red line represents analytically computed luminosity and therefore is not a fit!

The non-factorisation ratio is defined as "true" luminosity divided by "vdM" luminosity. For that reason the simulation mimicked the vdM procedure to obtain the luminosity by shifting the beams. Both simulated scans are in Fig. 6.9, 6.10. Important to note here is, that the fit is a single Gaussian, because both beams are modeled by single Gaussian. This may not hold true once other bunch models would be used. (Convolution of two single Gaussians make up one single Gaussian, but convolution of two double Gaussians makes four single Gaussians.) The analytical formula for "vdM" luminosity is in Eq. (6.10). But to obtain it from the simulation several steps have to be made. For each separation the "rate" is saved into a graph which is later fitted by the appropriate function. The fit is integrated and the ratio of head-on rate by the fit integral gives the resulting "vdM" luminosity.

$$L_{vdM*} = 2\pi\sqrt{(\sigma_{x1}^2 + \sigma_{x2}^2)(\sigma_{y1}^2 + \sigma_{y2}^2)}L_{true*}^2. \tag{6.10}$$
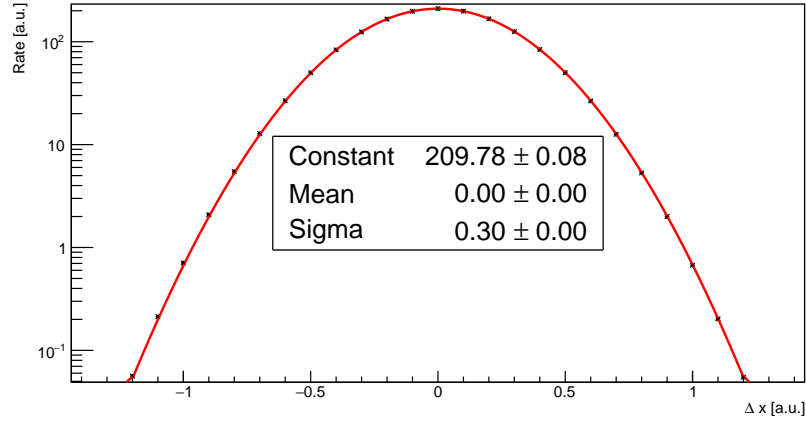


Figure 6.9: Simulation output demonstrating the $x$-scan of the vdM calibration. There are 25 scan points (black) fitted by a Gaussian function (red).
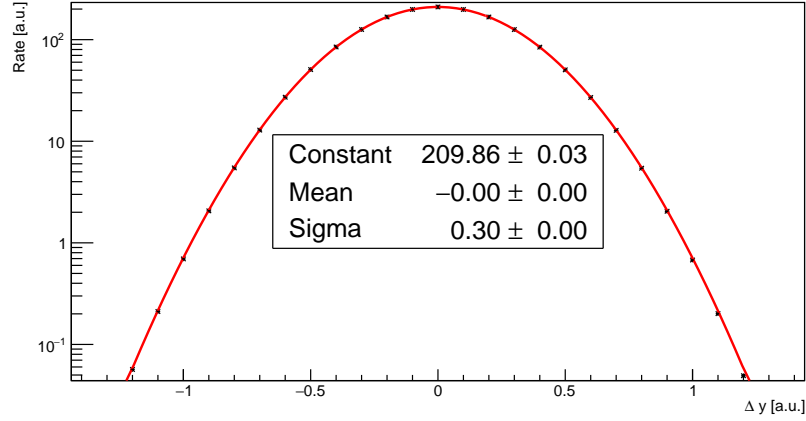
Figure 6.10: Simulation output demonstrating the $y$-scan of the vdM calibration. There are 25 scan points (black) fitted by a Gaussian function (red).

    With all this done, it is possible to compare results for the non-factorisation ratio $R = \frac{L_{true}}{L_{vdM}}$ . Figure 6.11 compares the pure simulation values (black) with the analytical prediction (red line). Note that the correction for non-factorisation effects can be quite large. The agreement between the results are well within the simulation uncertainty. The parameters of the simulation were the following: $\sigma_{x1} = 0.25$, $\sigma_{x2} = 0.2$, $\sigma_{y1} = 0.2$, $\sigma_{y2} = 0.25$, $\rho_2 = 0.3$ and $\rho_1$ was variable from -0.5 to 0.5. The maximum difference between analytically predicted value and the numerically obtained is less than 0.2% meaning that the uncertainty is overestimated for the chosen bunch parameters.
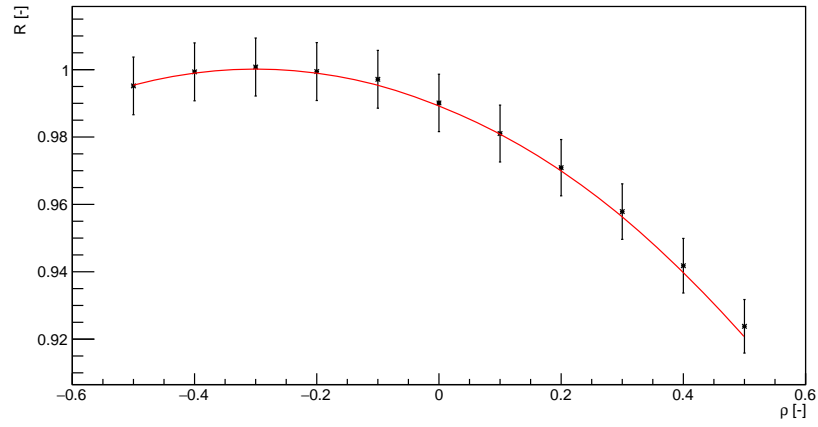
Figure 6.11: Non-factorisation ratio computed analytically (red line) and obtained by a simulation (black dots). The simulation results agree with the analytical prediction within the error.

# Chapter 7

# Simulation analysis

The previous chapter demonstrated the difference in the simulation of the measured luminosity compared to the one truly delivered. Now we will treat a more realistic case by adding finite detector resolution and measurement uncertainty. To do that ALICE real-life data from several vdM scans have been used. But first the approach used by ALICE will be presented. Second, the simulation mimicking real-life data will be explained. And last will be presented a study of uncertainties for this approach while using different models (single or double Gaussian).

## 7.1 ALICE approach

In Section 4.1.1 the method of obtaining an unconstrained primary vertex and appropriate covariance matrix has been sketched. This is the starting point for the following approach of bunch non-factorisation measurement. For each beam separation a luminosity region is reconstructed from all unconstrained primary vertices. The luminosity region is fitted by a single Gaussian, which takes into account the measurement uncertainty of each vertex. From the single Gaussian the mean, RMS value and correlation is extracted. These values are plotted with their dependence on the beam separation and fitted to a model which includes correlations, specifically a model with bunches described by double Gaussian distributions. The two double Gaussian distributions represent the colliding beams and the bunch parameters are set, by a minimisation procedure, such that the luminosity region exhibits the same behavior as that expected from the double Gaussian model. Figures representing this procedure (for the simulated data reported below) are shown in the appendix.

For the simulation we used parameters which correspond to those obtained in the analysis of real data. The data were acquired in pPb collisions with an energy of 8.16 TeV per nucleon pair, the fill number is 5533. After the two XY scans a length-scale calibration was executed. A selection of the data was performed, by picking vertices with more than 15 contributors (this enhances

Table 7.1: Values of double Gaussian model fitted to real-life data by Dr. Mayer.

| $w_1 = 0.64$ | | $w_2 = 0.44$ | |
|---|---|---|---|
| $\sigma_{x1a} = 36.6\ \mu m$ | $\sigma_{x1b} = 22.0\ \mu m$ | $\sigma_{x2a} = 39.7\ \mu m$ | $\sigma_{x2b} = 37.3\ \mu m$ |
| $\sigma_{y1a} = 23.5\ \mu m$ | $\sigma_{y1b} = 13.6\ \mu m$ | $\sigma_{y2a} = 26.5\ \mu m$ | $\sigma_{y2b} = 32.6\ \mu m$ |
| $\sigma_{z1a} = 84.0\ mm$ | $\sigma_{z1b} = 90.7\ mm$ | $\sigma_{z2a} = 85.0\ mm$ | $\sigma_{z2b} = 42.5\ mm$ |
| $\rho_{xy1a} = 0.16$ | $\rho_{xy1b} = 0.25$ | $\rho_{xy2a} = 0.26$ | $\rho_{xy2b} = $ -0.06 |

the resolution of the vertex position). Graphs in Fig.7.1, Fig.7.2 and Fig.7.3 display the dependence of the resolution on the vertex position (which are the diagonal terms in the covariance matrix). There are other terms which define the resolution correlations dependent on two coordinates. The fit was done by Dr. Christoph Mayer from the ALICE Collaboration[1]. The parameters found are reported in Table (7.1).

Every fitted parameter has an uncertainty of the determined value (in Table 7.1 the uncertainties are omitted, since they are not crucial for setting simulation input parameters). To obtain the non-factorisation ratio $R$ the fit values are used. The uncertainty of the ratio is then obtained by varying the parameters within their fit uncertainty and computing non-factorisation ratio again.
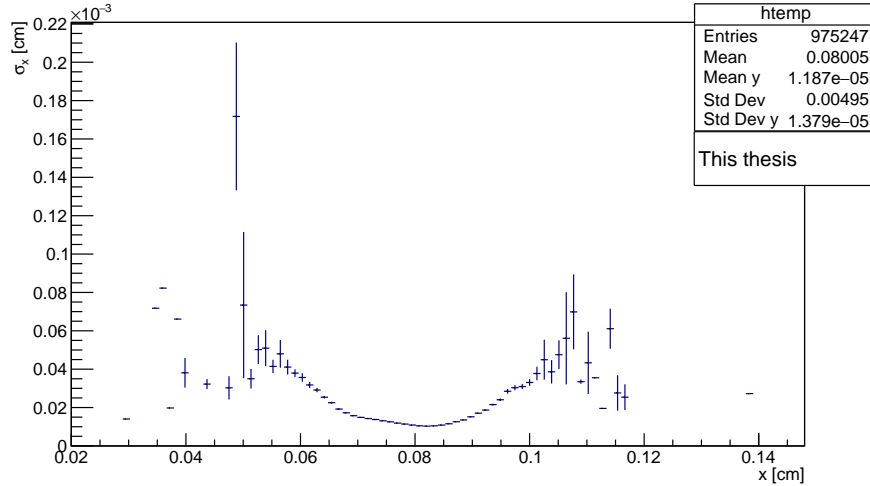


Figure 7.1: Dependence of the resolution on the vertex position in the $x$-direction. For the most part the resolution $\sigma_x$ is around 20 $\mu m$, which is comparable to the bunch width.

---

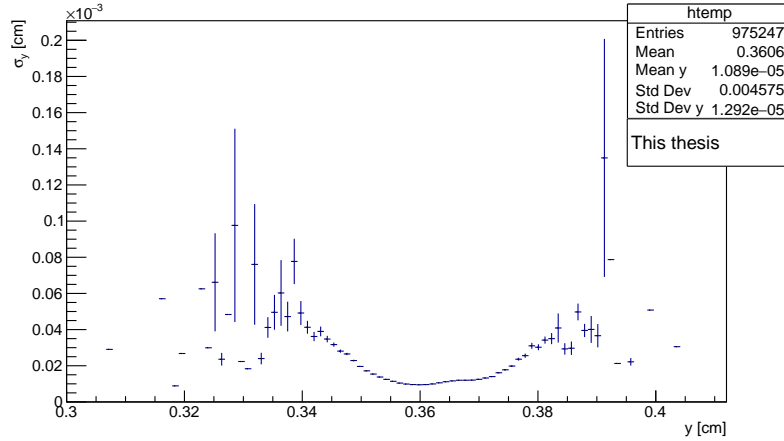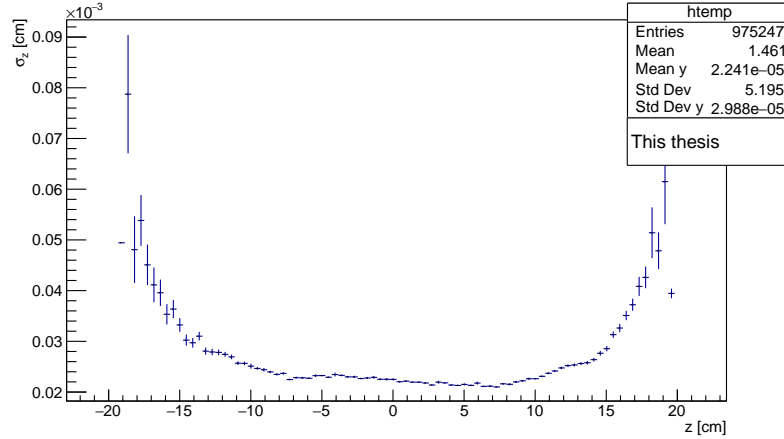[1] This was a personal communication between Dr. Mayer and Dr. Contreras, my supervisor.

Figure 7.2: Dependence of the resolution on the vertex position in the $y$-direction. For the most part the resolution $\sigma_y$ is around 20 $\mu m$, which is comparable to the bunch width.



Figure 7.3: Dependence of the resolution on the vertex position in the $z$-direction. For the most part the resolution $\sigma_z$ is around 30 $\mu m$, which is three orders of magnitude smaller than the bunch width.

## 7.2    Vertex simulation description

In Chapter 6 the part of simulation computing luminosity for various collision conditions has been presented. In order to obtain the vertices, similar input parameters to the real ones are used for the bunch distributions. Once the histogram with the luminosity region is obtained a proportional part of points to the number of entries is randomly generated. These points represent the vertices. Covariance matrices from real-life data are randomly assigned and the generated vertices are smeared. This step usually doubles the RMS of the luminosity region, however, since the error matrices are kept, it is possible to "unfold" the smearing and obtain the input parameters.

To better illustrate the process described earlier, two figures are shown. Figure 7.4 shows generated transverse vertex distribution directly from the simulation. Whereas Fig. 7.5 displayes the same distribution of vertices smeared by covariance matrices.
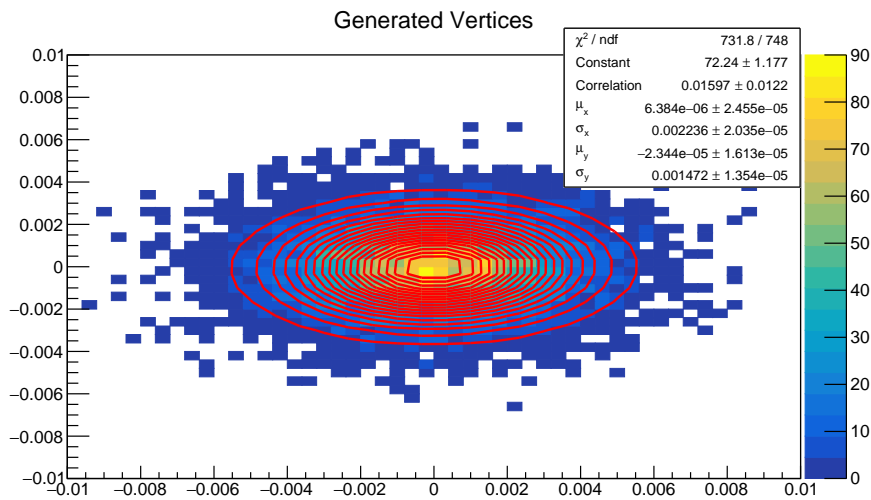


Figure 7.4: Transverse vertex distribution generated by the simulation, the $x$ and $y$ axis represent the vertex positions in arbitrary units. Red curves present 2D Gaussian fit.
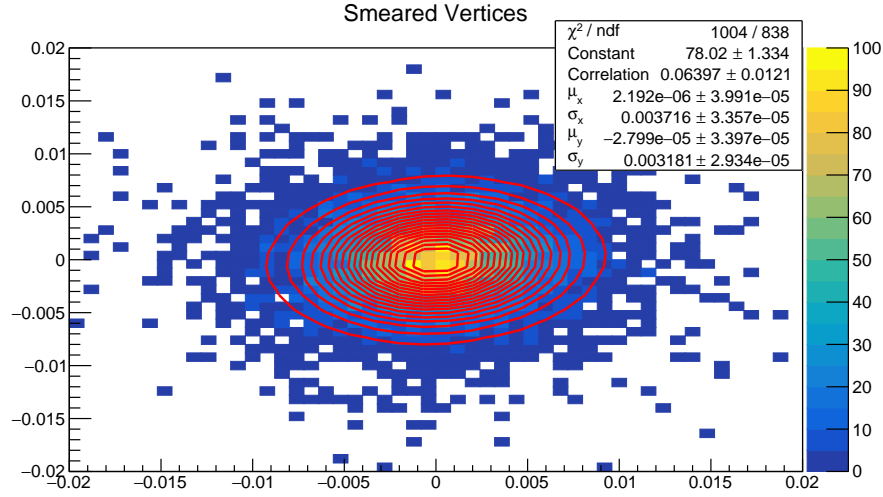
Figure 7.5: Transverse vertex distribution originating from previous figure, vertices are randomly shifted by a covariance matrix obtained by real-life data, the $x$ and $y$ axis represent the vertex positions in arbitrary units.

## 7.3    Analysis of simulated data

The assignment was simple – compare the simulation input values with those acquired by the analysis. However, there are many possible configurations and aspects that can be tested. For that reason, only cases closely related to the LHC are studied. The following list gives a brief overlook of the configurations chosen to be presented:

1. Varying the bunch width in one direction, while keeping others constant.

2. Varying the correlation in one bunch.

3. Analysing single Gaussian bunch collisions with a double Gaussian model.

4. Analysing double Gaussian bunch collisions with a single Gaussian model.

Complete figures of fits can be found in the appendix. The last possible configuration of analysing double Gaussian collisions with double Gaussian model is ongoing and thus the results are not shown in this thesis.

**1.** In the single Gaussian model, there are two bunch widths in the transverse plane. First only one was varied on input and the dependence of output value on input was created. To make sure, that the other widths are not affected by

the change of the one, their fitted value was also added into the Fig. 7.6. Even though smeared vertices were used, the parameters obtained were very close to the ones that were input. The average uncertainty was 0.4%, which is even lower, than the uncertainty of the simulated luminosity compared to the analytically computed from the parameters. Next step was to change two bunch widths simultaneously – the bunch width in $y$-direction was decreased while the width in $x$-direction was increased. The result is presented in Fig. 7.7. The uncertainty has increased slightly, but it is still very precise – 0.6%. It is important to note, that to find the bunch widths the correlation factors were fixed to zero. Detailed fits are in appendix, see Fig. A.1-A.3. Note that all parameters are correctly recovered by the fitting procedure. That the fit provides a reasonable value of $\chi^2$ and that, as it should be in this case, the correction factor for non-factorisation effects (denoted by R in Fig. A.1) is 1.0, meaning no correction is needed. The conclusion of this exercise is that the method used by ALICE (and also by ATLAS) works correctly in this case.
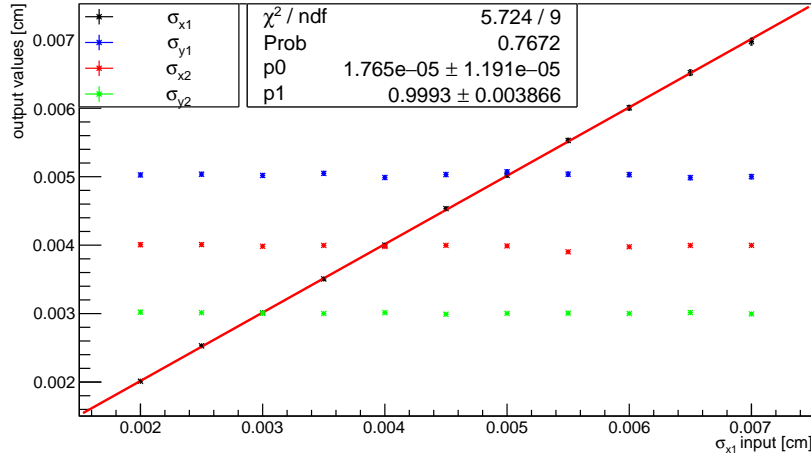


Figure 7.6: Dependence of bunch widths obtained by the analysis software on the input value of $\sigma_{x1}$ - bunch width in $x$ direction of the first beam. Results for the single Gaussian model of the bunch profiles.
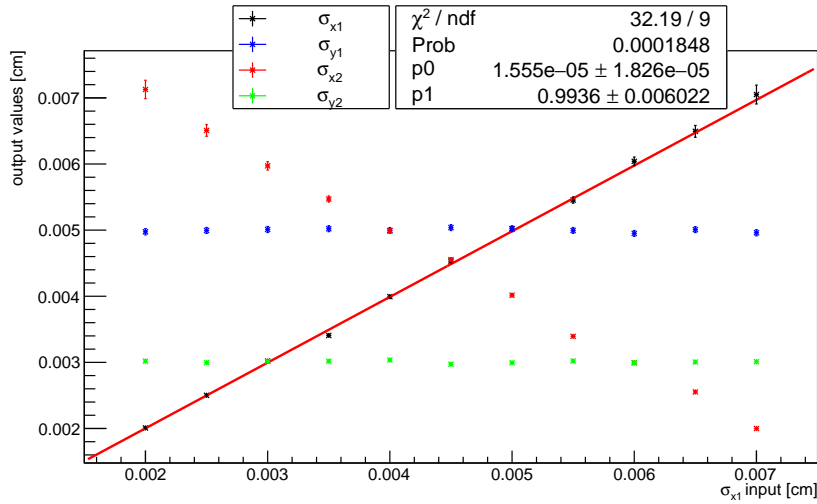
Figure 7.7: Dependence of bunch widths obtained by the analysis software on the input value of $\sigma_{x1}$ - bunch width in $x$ direction of the first beam. Results for the single Gaussian model of the bunch profiles, fitted by a single Gaussian model.

**2.**   To obtain the correct value of the non-factorisation ratio, the correct value of the bunch correlation has to be extracted. The same approach was chosen as in 1. − the dependence of the value obtained by the analysis was compared to the input value. First with one beam having the correlation equal to zero and later a non-zero constant value. Figure 7.8 shows the mentioned dependence, representing a more complex case. Again the uncertainty is very low, around 0.3%. It was shown, that it is possible to obtain parameters very close to those from the input. But the key thing is, whether the non-factorisation ratio is reliable. The highest actual difference between the analytical calculation from input parameters and those given by the analysis software is 0.1% (although the uncertainty is in some cases higher) as can be seen from Fig. 7.9. The detailed fits are Fig. A.4-A.6
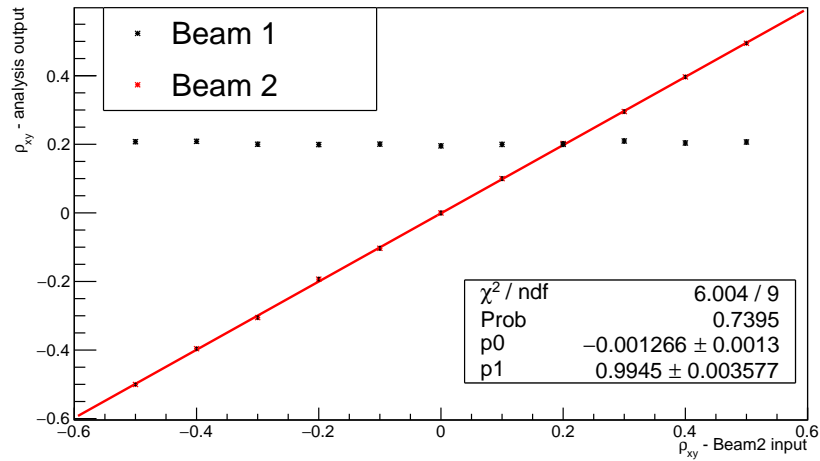
Figure 7.8: Analysis of correlation factor for different input values. Results for the single Gaussian model of the bunch profiles, fitted by a single Gaussian model.
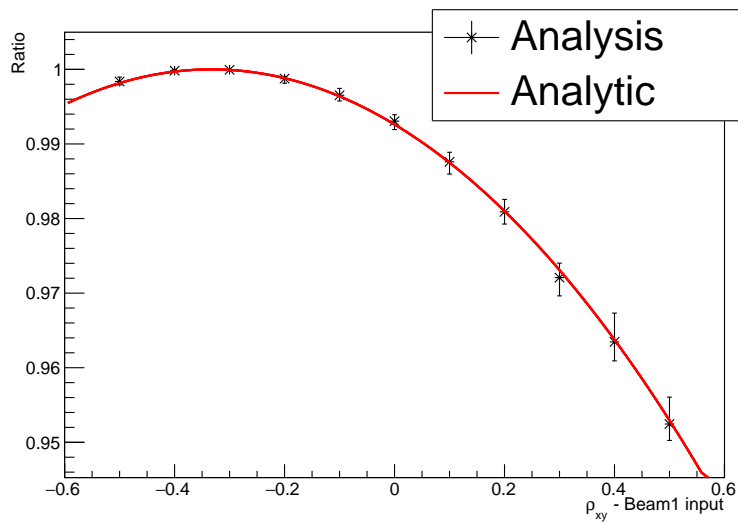


Figure 7.9: Analysis of non-factorisation ratio for different input values. Results for the single Gaussian model of the bunch profiles, fitted by a single Gaussian model.

**3.** For the vdM scan, a great amount of work from the LHC side is put into making the bunches as close to a single Gaussian distribution as possible. However, from the analysis point of view, the fit with double Gaussian distributions is more sensitive to non-factorisation effects. The natural question that arises is, if the non-factorisation ratio is assigned correctly for bunches that are real single Gaussians when the fitting is done with double Gaussian bunches. There are more than 2 times more parameters which have to be correctly fitted and due to the double Gaussian symmetry of the Gaussians, the minimising is sometimes problematic. The non-factorisation ratio dependent on the correlation factor is presented in Fig. 7.10. The main difference between this approach and the one presented earlier is the size of the uncertainties. This is exactly due to the larger number of parameters, which can substitute one another in the case of single Gaussian collisions. This creates a larger uncertainty of each parameter and subsequently has an effect on the uncertainty. The detailed fits in appendix are Fig. A.7-A.12. Note that the parameter $w$ is very close to either 0 or 1, so the person doing this particular analysis, when checking the values of the parameters, should realise that a single Gaussian model may be more adequate and try also that option.
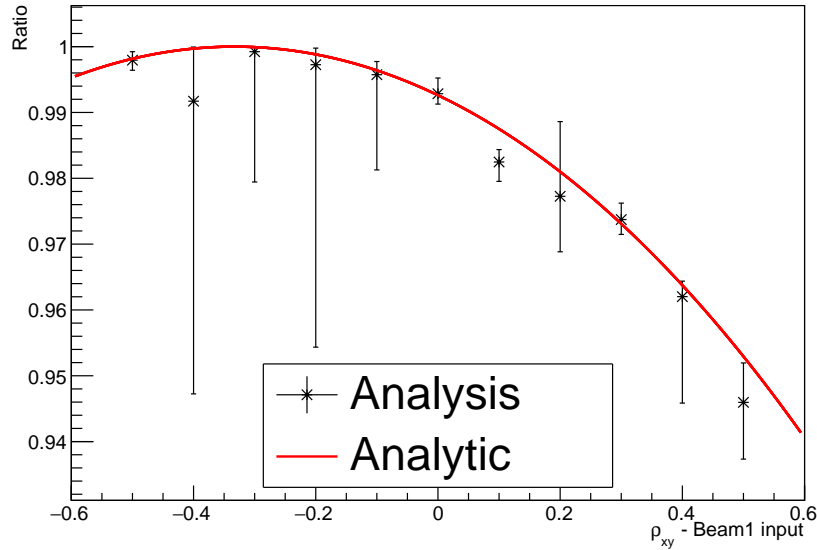


Figure 7.10: Non-factorisation ratio dependent on correlation factor of the first beam. Results for the single Gaussian model of the bunch profiles, fitted by a double Gaussian model.

**4.**  As has been presented in paragraph 2, the single Gaussian model is performing fairly well.  Could it also evaluate correctly the non-factorisation of double Gaussian collisions?  Before going to the results of the simulation, let's make a thought experiment.  If the double Gaussian has the weight $w = 0.5$ and the same widths for both parts but the opposite sign of correlation factors, the fit of single Gaussian would not find any correlation at all.  And this has an effect on the overall luminosity and the non-factorisation ratio.  Figure 7.11 presents the analytical ratio computed from a double Gaussian model and the points are simulated by fitting with a single Gaussian model.  The whole set of parameters used to generate the simulated data is:

| | | | |
|---|---|---|---|
| $w_1 = 0.64$ | | $w_2 = 0.44$ | |
| $\sigma_{x1a} = 36.6\ \mu m$ | $\sigma_{x1b} = 22.0\ \mu m$ | $\sigma_{x2a} = 39.7\ \mu m$ | $\sigma_{x2b} = 37.3\ \mu m$ |
| $\sigma_{y1a} = 23.5\ \mu m$ | $\sigma_{y1b} = 13.6\ \mu m$ | $\sigma_{y2a} = 26.5\ \mu m$ | $\sigma_{y2b} = 32.6\ \mu m$ |
| $\sigma_{z1a} = 75.0\ mm$ | $\sigma_{z1b} = 70.0\ mm$ | $\sigma_{z2a} = 75.0\ mm$ | $\sigma_{z2b} = 71.0\ mm$ |
| $\rho_{xy1a} = x.xx$ | $\rho_{xy1b} = 0.25$ | $\rho_{xy2a} = 0.26$ | $\rho_{xy2b} = -0.06$ |

which is comparable to the real-life data, the $\rho_{xy1a}$ was changed to see the impact on the non-factorisation ratio.  However, the single Gaussian model wasn't able to reproduce the analytically computed values.  The most probable explanation arises from the thought experiment.  The detailed fits are in the appendix as Fig. A.13-A.15.
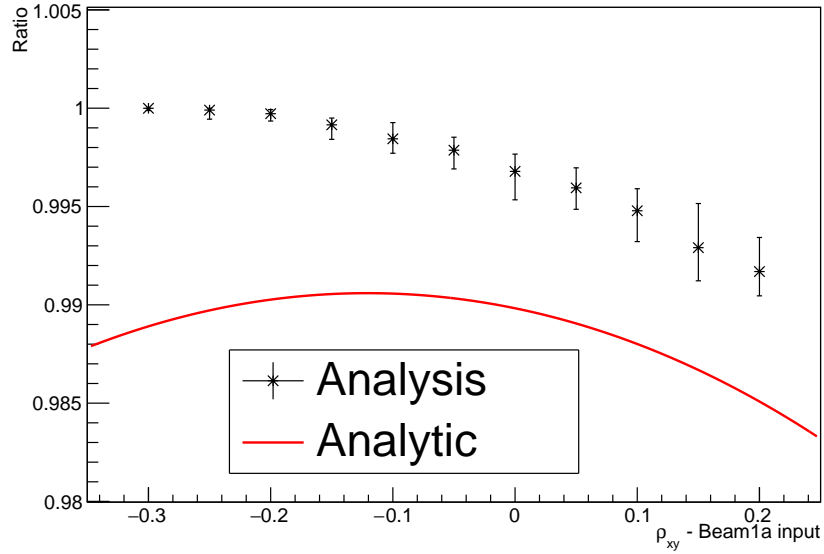
Figure 7.11: Dependence of non-factorisation ratio on correlation factor using Double Gaussian model for generating data and Single Gaussian model for the analysis. Red is analytical prediction for the input data and black are points obtained from the analysis.

# Chapter 8

# Conclusion

Determination of luminosity via van der Meer scans has been presented. The ALICE experiment has been briefly introduced and key detectors to luminosity measurement were presented. The method of estimating non-factorisation by fitting the luminosity region provided by the measurement of primary vertices has been described. To understand non-factorisation further a simulation has been developed. The simulation is capable of using different bunch distributions to create a luminosity region. The luminosity regions are later smeared with real-life data (uncertainties of measurement) and the ALICE analysis software is used to obtain the individual bunch parameters.

Taking into account that the simulation can generate non-factorisation with a precision of 0.2%, the analysis code is able to approach similar values for single Gaussian model, although the determined uncertainty (by the analysis software) is (for some cases) higher. An analysis of single Gaussian bunches by double Gaussian model was also carried out. The results are consistent with analytical predictions, however, the uncertainties are far larger. On the other hand, it is expected that the analyser would notice the large uncertainties of parameters and would try to use single Gaussian model instead. The single Gaussian model was also used to analyse double Gaussian bunch profiles. In that case the output was away from analytical predictions and the uncertainties were smaller than the distance from the analytic predictions. But the data were obviously not fitted correctly as can be seen from Fig. A.14-A.15, so an analyser would know that something is not correct.

The testing of double Gaussian bunches analysed with double Gaussian model is in progress and cannot be shown in this thesis. Another step is to benchmark collisions under crossing angle and compare the results to analytical predictions (which were not explicitly computed in this thesis). The usage of other distributions to generate vertices would be a future goal. The program can be also used to optimise other aspects of the vdM scan procedure. For example, the amount of time that the rate is measured in each step: right now the same time is spent in each step, which does not look like an optimal setup; or to optimise the size of steps during the scan: currently all steps are of the same lenght, which also seems not to be optimal to perform the integrals in Eq. (3.7).

# Bibliography

[1] Gabriel Anders. *Absolute luminosity determination for the ATLAS experiment.* PhD thesis, CERN, 2013. URL: `http://inspirehep.net/record/1296442/files/525947540_CERN-THESIS-2013-111.pdf`.

[2] Arturo Tauro. ALICE Schematics. General Photo, May 2017. URL: `http://cds.cern.ch/record/2263642`.

[3] Betty Bezverkhny Abelev et al. Measurement of visible cross sections in proton-lead collisions at $\sqrt{s_{NN}} = 5.02$ TeV in van der Meer scans with the ALICE detector. *JINST*, 9(11):P11003, 2014. `arXiv:1405.1849`, `doi:10.1088/1748-0221/9/11/P11003`.

[4] Mikhail Zobov. Crab Waist collision scheme: a novel approach for particle colliders. *J. Phys. Conf. Ser.*, 747(1):012090, 2016. `arXiv:1608.06150`, `doi:10.1088/1742-6596/747/1/012090`.

[5] R. B. Palmer. Energy Scaling, Crab Crossing, and the Pair Problem. *eConf*, C8806271:613–619, 1988.

[6] Rama Calaga, Ofelia Capatina, and Giovanna Vandoni. The SPS Tests of the HL-LHC Crab Cavities. In *Proceedings, 9th International Particle Accelerator Conference (IPAC 2018): Vancouver, BC Canada*, page TU-PAF057, 2018. `doi:10.18429/JACoW-IPAC2018-TUPAF057`.

[7] Jan Pucek. Stanovení luminozity v experimentu ALICE. Bachelor's Thesis, FNSPE, 2017.

[8] S. van der Meer. Calibration of the Effective Beam Height in the ISR. 1968.

[9] C. Rubbia. Measurement of the Luminosity of p anti-p Collider with a (Generalized) Van Der Meer Method. 1977.

[10] CMS luminosity measurement for the 2015 data-taking period. Technical Report CMS-PAS-LUM-15-001, CERN, Geneva, 2017. URL: `https://cds.cern.ch/record/2138682`.

[11] Roel Aaij et al. Precision luminosity measurements at LHCb. *JINST*, 9(12):P12005, 2014. `arXiv:1410.0149`, `doi:10.1088/1748-0221/9/12/P12005`.

[12] P Odier, M Ludwig, and S Thoulet. The DCCT for the LHC Beam Intensity Measurement. Technical Report CERN-BE-2009-019, CERN, Geneva, May 2009. URL: `https://cds.cern.ch/record/1183400`.

[13] D Belohrad, O R Jones, M Ludwig, J J Savioz, and S Thoulet. Implementation of the Electronics Chain for the Bunch by Bunch Intensity Measurement Devices for the LHC. Technical Report CERN-BE-2009-018, CERN, Geneva, May 2009. URL: `https://cds.cern.ch/record/1183399`.

[14] Fabienne Marcastel. ALICE brochure (English version). Brochure ALICE (version anglaise). Jul 2014. URL: `https://cds.cern.ch/record/1965941`.

[15] Betty Bezverkhny Abelev et al. Performance of the ALICE Experiment at the CERN LHC. *Int. J. Mod. Phys.*, A29:1430044, 2014. `arXiv:1402.4476`, `doi:10.1142/S0217751X14300440`.

[16] Samuel Nathan Webb. *Factorisation of beams in van der Meer scans and measurements of the $\phi_\eta^*$ distribution of $Z \to e^+e^-$ events in pp collisions at $\sqrt{s} = 8$ TeV with the ATLAS detector.* PhD thesis, Manchester U., 2015-06-01. URL: `http://inspirehep.net/record/1381312/files/CERN-THESIS-2015-054.pdf`.

[17] R. Brun and F. Rademakers. ROOT: An object oriented data analysis framework. *Nucl. Instrum. Meth.*, A389:81–86, 1997. `doi:10.1016/S0168-9002(97)00048-X`.

# Appendix A

# Selected analysis fits

This part of appendix has the goal of showing more details of fitting analysis. The introduction into this method is in Sec. 7.1. The selection will pick best and worst case in the data since there are usually around 11 sets of 14 fits performed to create a figure such as Fig 7.6. The fits will be presented in the same order as they were in the thesis.

## Sigma fits

First of all, the bunch width was varied and the output width was studied. The output had exceptional precision given that the data was smeared. Even when the correlation factors were not fixed during the fitting procedure, the uncertainty was around 0.6%.

$\sigma_{1a}^X$ = 50.2±0.3 μm

$\sigma_{1a}^Y$ = 50.7±0.3 μm

$\sigma_{1a}^Z$ = 5.0±0.0 cm

$\rho_{1a}^{XY}$ = 0.00±0.01

$\sigma_{2a}^X$ = 39.9±0.2 μm

$\sigma_{2a}^Y$ = 30.0±0.1 μm

$\sigma_{2a}^Z$ = 5.0±0.0 cm

$\rho_{2a}^{XY}$ = -0.00±0.01

$\alpha^{XZ}$ = 0.0±0.0 μrad

$\alpha^{YZ}$ = 0.0±0.0 μrad

R = 1.000$^{+0.000}_{-0.000}$

$\chi^2$/NDF = 260/341=0.8

Figure A.1: The output parameters of the two single Gaussian bunches. The input parameters were: $\sigma_{1a}^x = 50$ μm, $\sigma_{1a}^y = 50$ μm, $\sigma_{2a}^x = 40$ μm, $\sigma_{2a}^y = 30$ μm, $\sigma_{1,2a}^z = 5$ cm, $\rho_{1,2a}^{xy} = 0$.
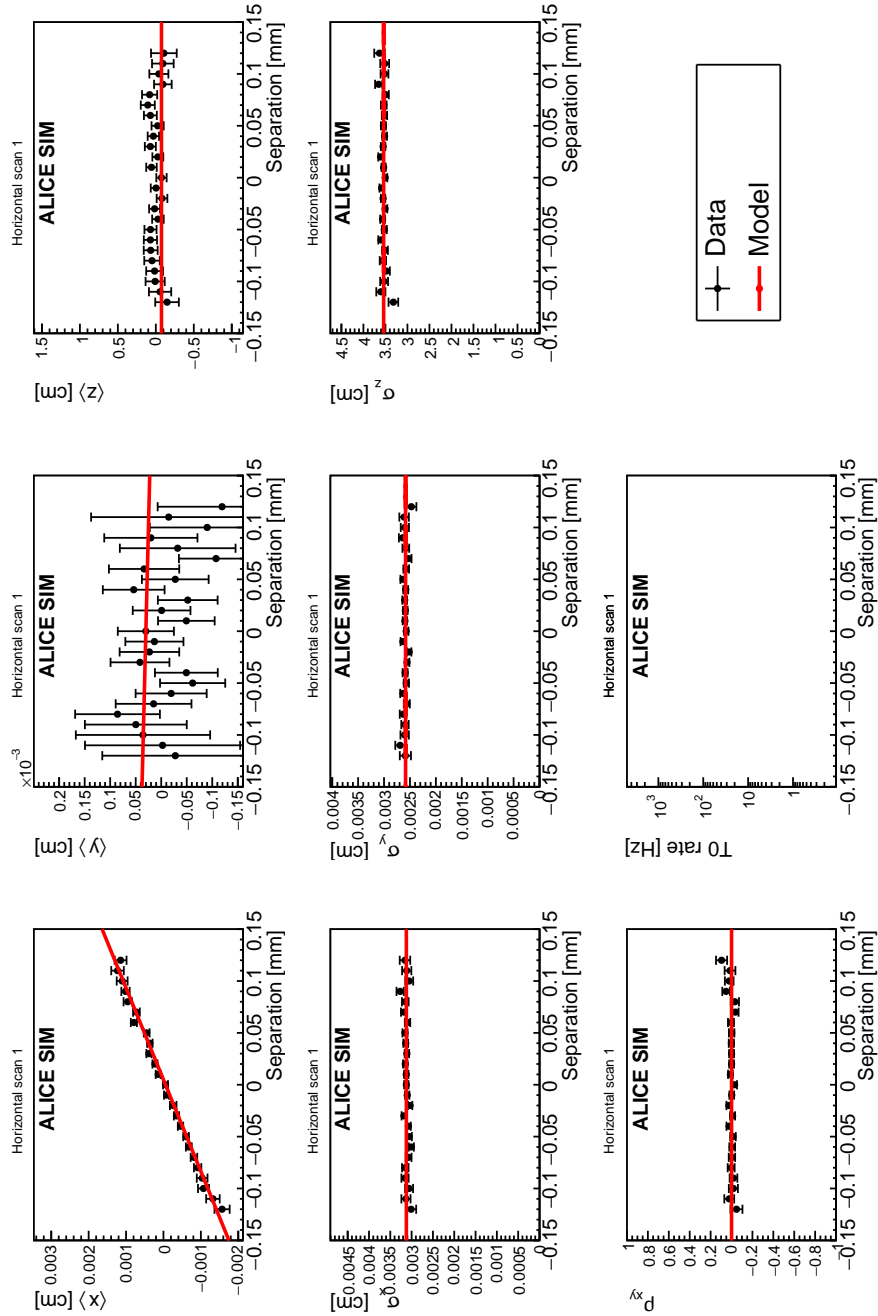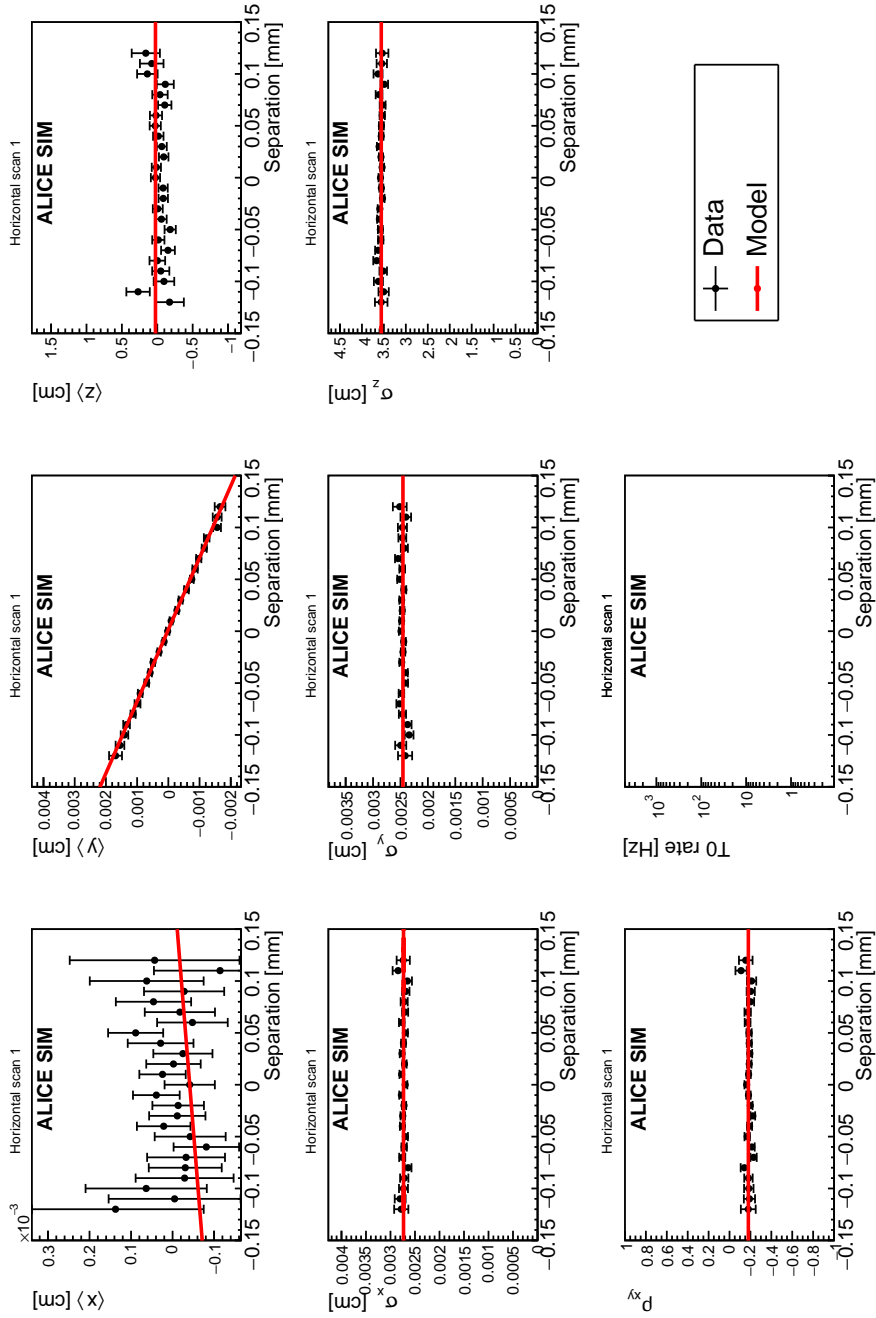
Figure A.2: The individual graphs and fits in the simulated vdM $x$-scan.
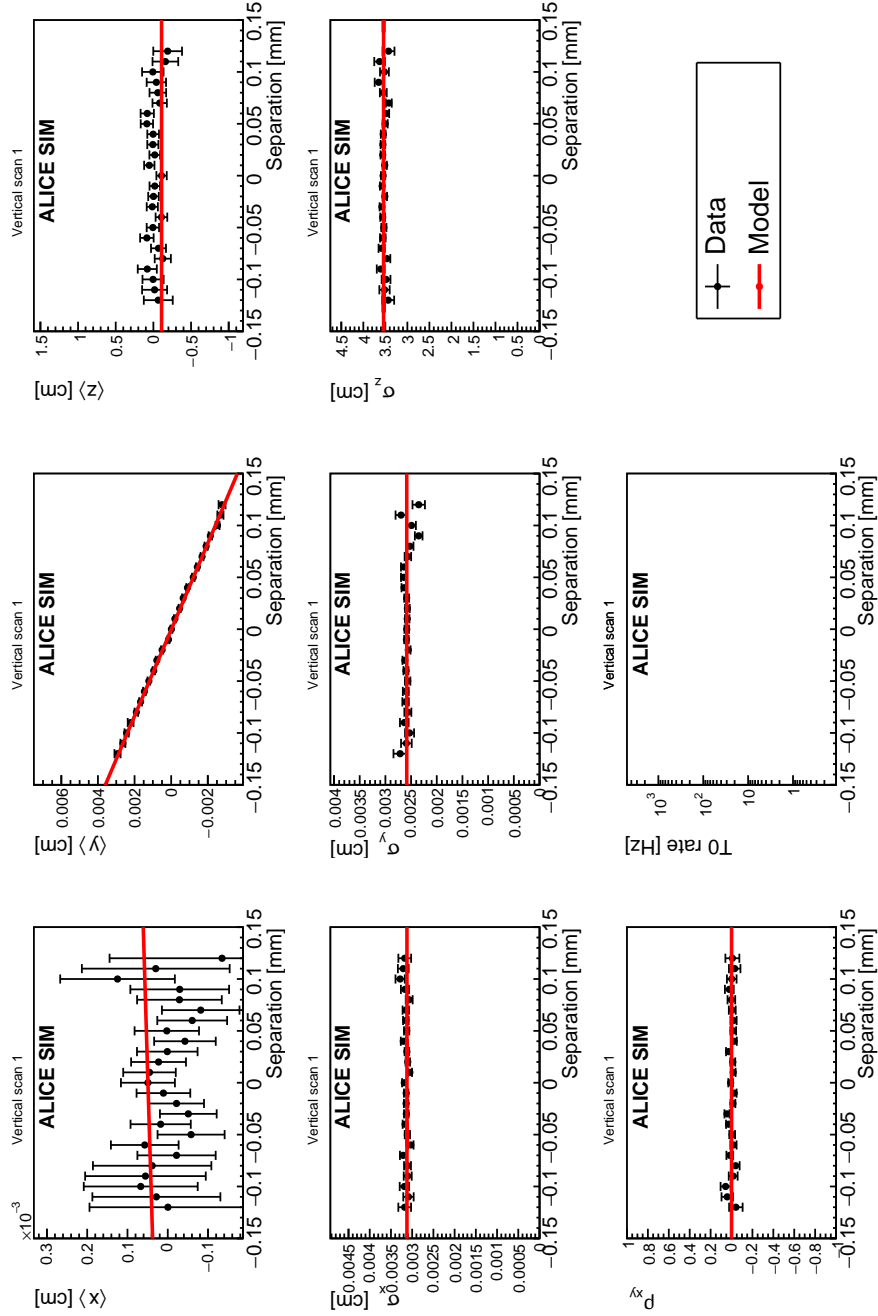
Figure A.3: The individual graphs and fits in the simulated vdM *y*-scan.

## Correlation factor and non-factorisation ratio fits

These fits were performed on the same set of data, only different quantities were monitored. The only difference was between individual points the uncertainty. For that reason, we show only one of the fit samples.

$\sigma^X_{1a}$ = 40.0±0.2 µm

$\sigma^Y_{1a}$ = 50.3±0.3 µm

$\sigma^Z_{1a}$ = 5.0±0.0 cm

$\rho^{XY}_{1a}$ = 0.21±0.01

$\sigma^X_{2a}$ = 40.3±0.2 µm

$\sigma^Y_{2a}$ = 30.2±0.1 µm

$\sigma^Z_{2a}$ = 5.0±0.0 cm

$\rho^{XY}_{2a}$ = -0.40±0.00

$\alpha^{XZ}$ = 0.0±0.0 µrad

$\alpha^{YZ}$ = 0.0±0.0 µrad

R = 1.000$^{+0.000}_{-0.000}$

$\chi^2$/NDF = 189/341=0.6

Figure A.4: The output parameters of the two correlated single Gaussian bunches. The input parameters were: $\sigma^x_{1a} = 40$ µm, $\sigma^y_{1a} = 50$ µm, $\sigma^x_{2a} = 40$ µm, $\sigma^y_{2a} = 30$ µm, $\sigma^z_{1,2a} = 5$ cm, $\rho^{xy}_{1a} = 0.2$, $\rho^{xy}_{1a} = -0.4$.
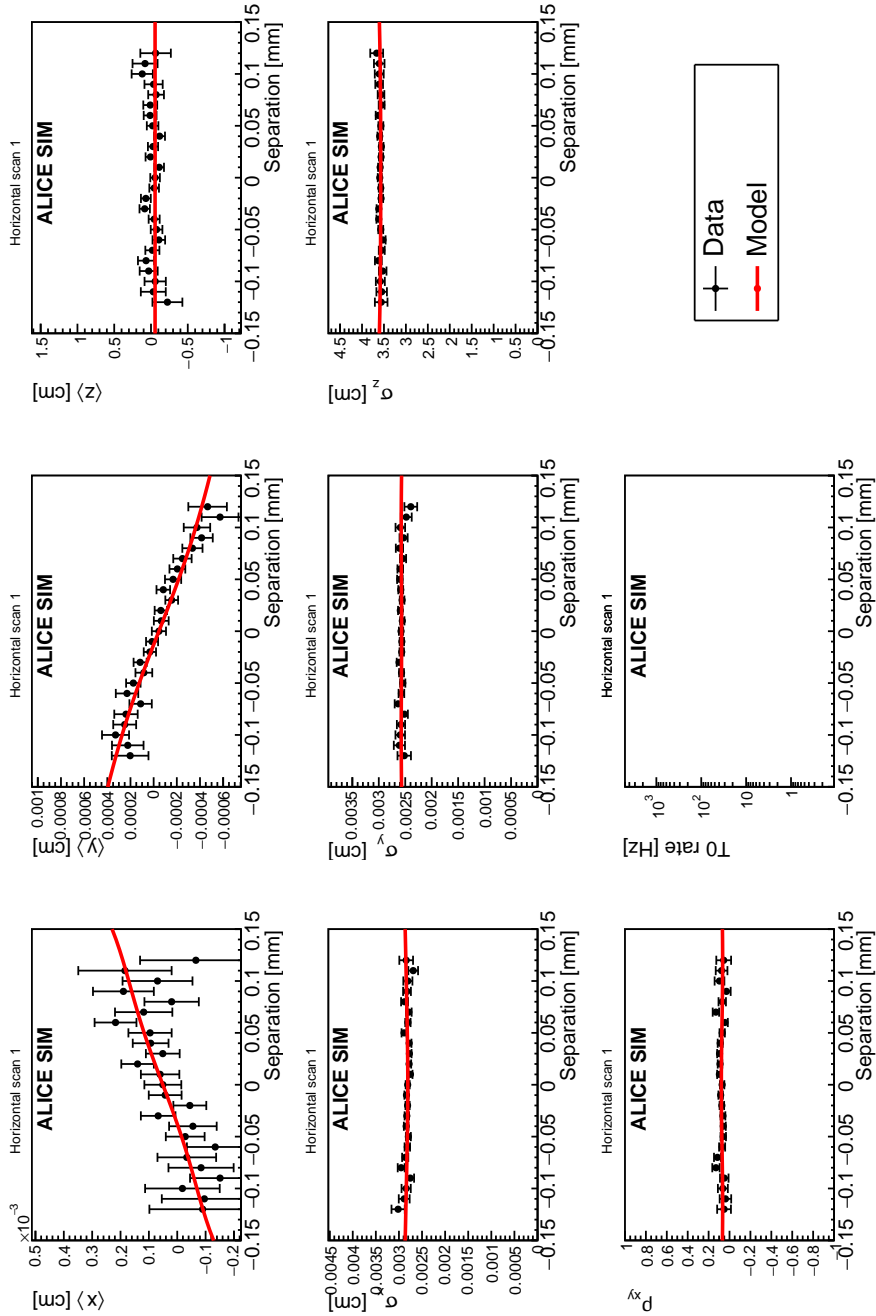
Figure A.5: The individual graphs and fits in the simulated vdM $x$-scan.
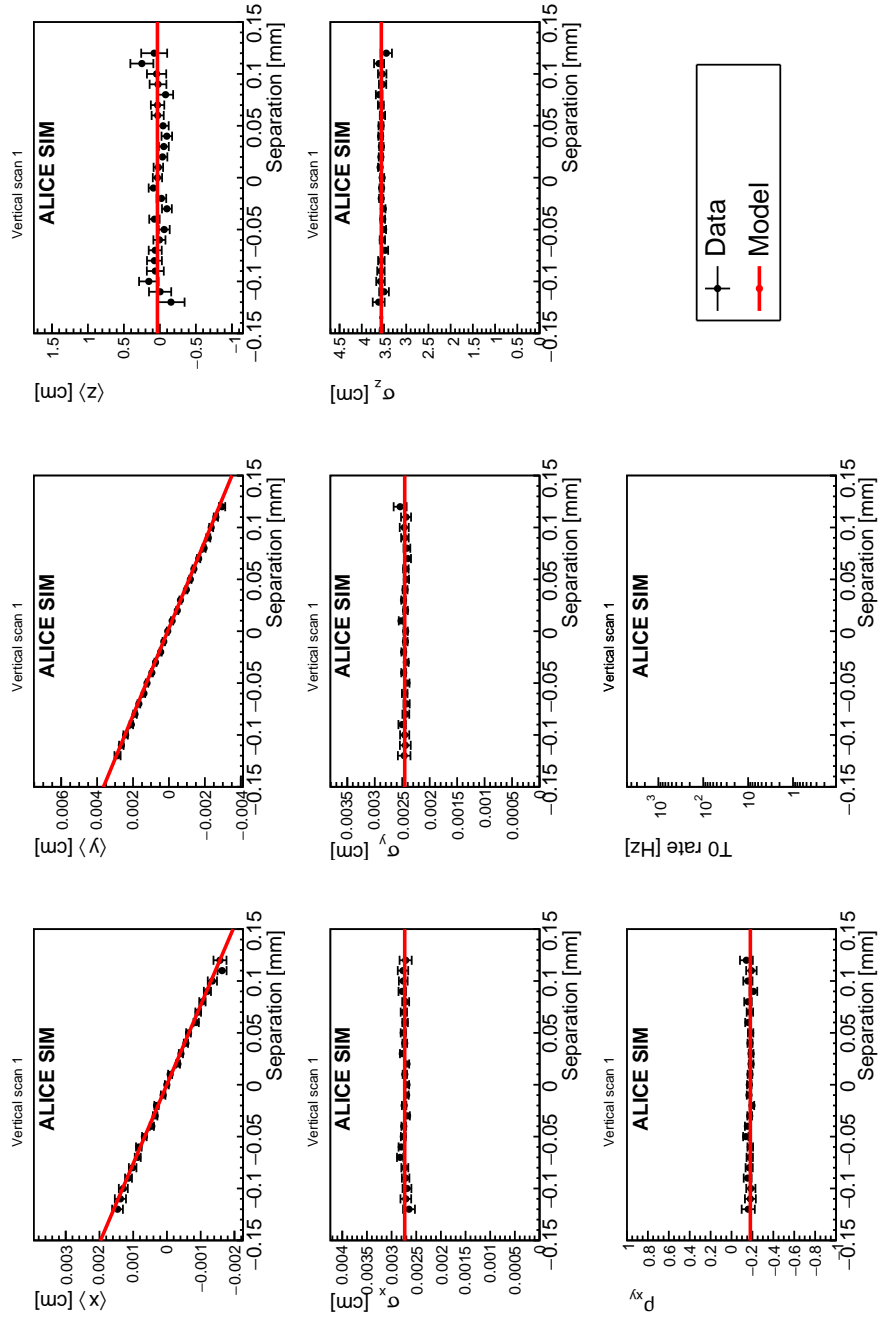
Figure A.6: The individual graphs and fits in the simulated vdM $y$-scan.

## Fitting by double Gaussian

The large uncertainties were caused mostly by parameters fitted too loosely. It is assumed that the person responsible for the analysis would find the weights close to 0 or 1 and would also try fitting with single Gaussian model with higher precision. The best fit is presented first and one of the more problematic ones is presented second.

$\sigma^X_{1a}$ = 37.8±0.2 μm     $S^X_{1b}$ = 1.06±0.00          $\sigma^X_{2a}$ = 39.8±0.2 μm     $S^X_{2b}$ = 1.15±0.05

$\sigma^Y_{1a}$ = 45.3±0.3 μm     $S^Y_{1b}$ = 1.11±0.01          $\sigma^Y_{2a}$ = 30.7±0.1 μm     $S^Y_{2b}$ = 0.75±1.34

$\sigma^Z_{1a}$ = 5.7±0.0 cm      $S^Z_{1b}$ = 0.84±0.00          $\sigma^Z_{2a}$ = 5.1±0.0 cm      $S^Z_{2b}$ = 1.42±0.06

$\rho^{XY}_{1a}$ = 0.90±1.36      $\rho^{XY}_{1b}$ = 0.18±0.01    $\rho^{XY}_{2a}$ = -0.00±0.01    $\rho^{XY}_{2b}$ = 0.07±0.08

$w_1$ = 0.01±0.00                                               $w_2$ = 0.92±0.01

$\alpha^{XZ}$ = 0.0±0.0 μrad

$\alpha^{YZ}$ = 0.0±0.0 μrad

$R = 0.993^{+0.002}_{-0.002}$

$\chi^2$/NDF = 176/331=0.5

Figure A.7: The output parameters of the two single Gaussian bunches fitted by double Gaussian model. The input parameters were: $\sigma^x_{1a} = 40$ μm, $\sigma^y_{1a} = 50$ μm, $\rho^{xy}_{1a} = 0.2$, $\sigma^x_{2a} = 40$ μm, $\sigma^y_{2a} = 30$ μm, $\sigma^z_{1,2a} = 5$ cm, $\rho^{xy}_{1a} = 0.0$.

Figure A.8: The individual graphs and fits in the simulated vdM $x$-scan.
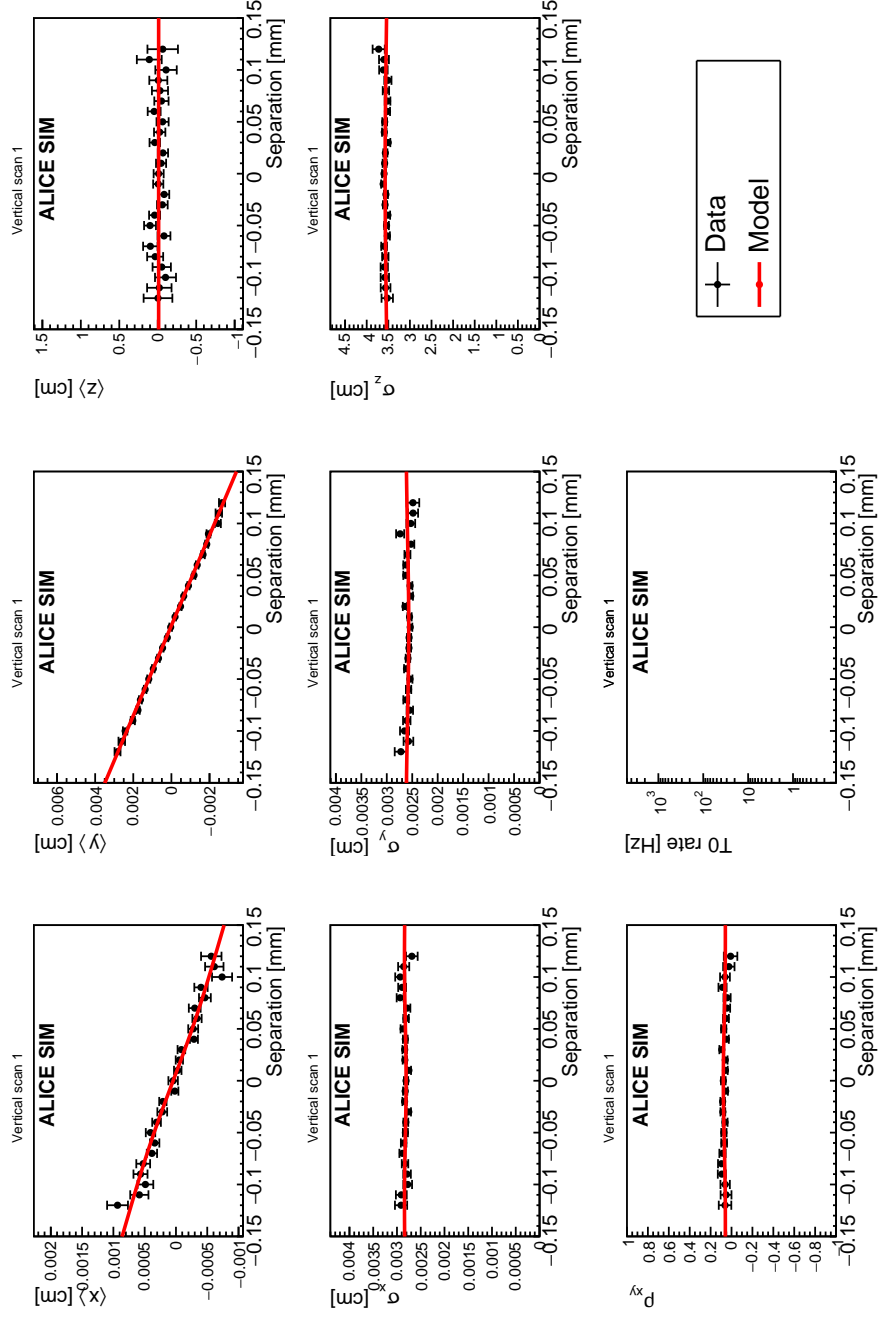
Figure A.9: The individual graphs and fits in the simulated vdM $y$-scan.

$\sigma^X_{1a}$ = 53.4±0.3 μm    $S^X_{1b}$ = 0.75±0.20         $\sigma^X_{2a}$ = 39.7±1.1 μm    $S^X_{2b}$ = 1.06±0.06

$\sigma^Y_{1a}$ = 48.6±0.4 μm    $S^Y_{1b}$ = 1.04±0.01         $\sigma^Y_{2a}$ = 30.5±0.7 μm    $S^Y_{2b}$ = 0.96±0.10

$\sigma^Z_{1a}$ = 7.0±2.2 cm     $S^Z_{1b}$ = 0.75±0.15         $\sigma^Z_{2a}$ = 3.8±0.7 cm     $S^Z_{2b}$ = 1.84±0.31

$\rho^{XY}_{1a}$ = -0.84±0.24    $\rho^{XY}_{1b}$ = 0.23±0.02   $\rho^{XY}_{2a}$ = -0.37±0.06   $\rho^{XY}_{2b}$ = -0.48±0.04

$w_1$ = 0.02±0.03                                             $w_2$ = 0.66±0.77

$\alpha^{XZ}$ = 0.0±0.0 μrad

$\alpha^{YZ}$ = 0.0±0.0 μrad

$R = 0.992^{+0.008}_{-0.044}$

$\chi^2$/NDF = 186/331=0.6

Figure A.10: The output parameters of the two single Gaussian bunches fitted by double Gaussian model. The input parameters were: $\sigma^x_{1a} = 40$ μm, $\sigma^y_{1a} = 50$ μm, $\rho^{xy}_{1a} = 0.2$, $\sigma^x_{2a} = 40$ μm, $\sigma^y_{2a} = 30$ μm, $\sigma^z_{1,2a} = 5$ cm, $\rho^{xy}_{1a} = -0.4$.
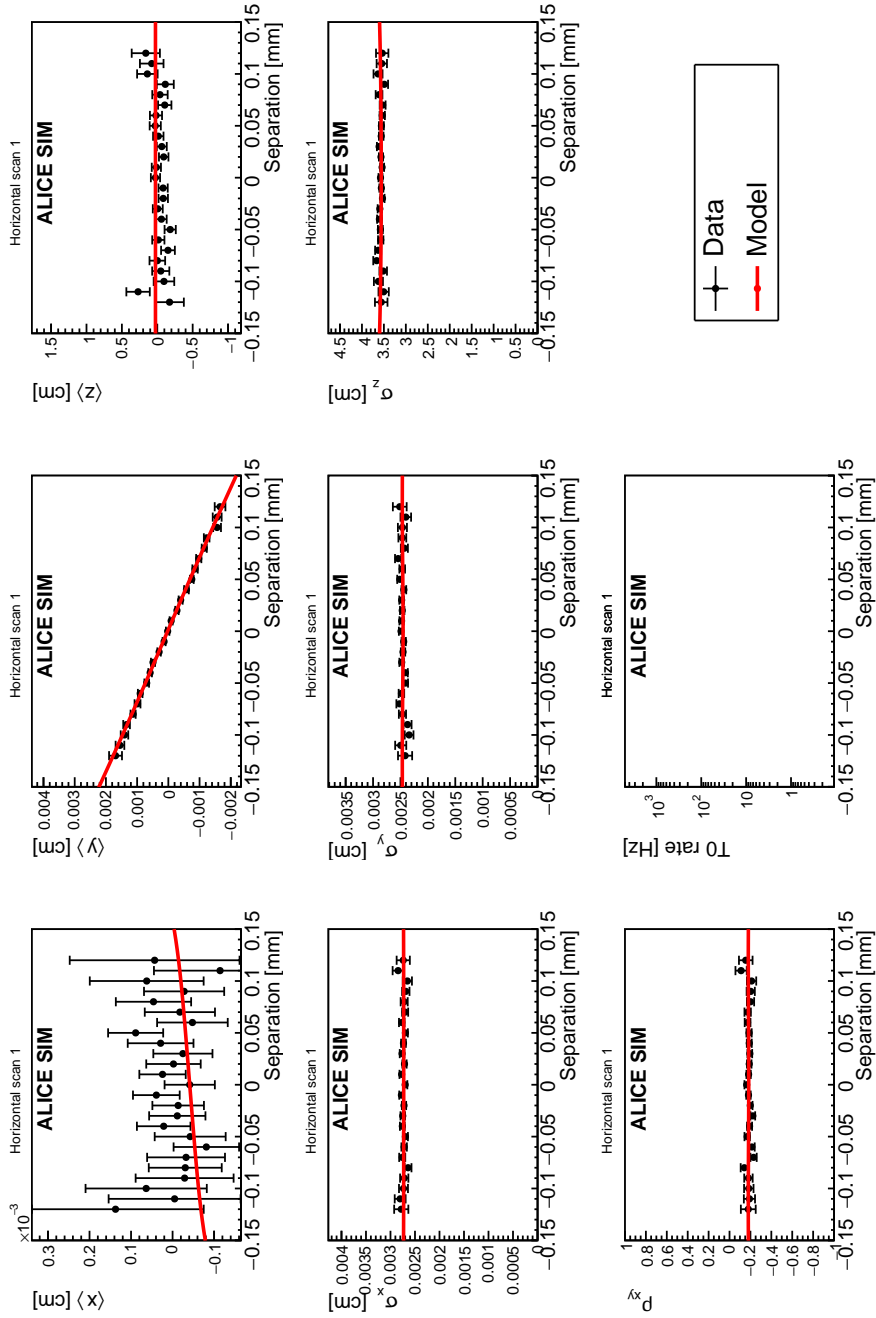
Figure A.11: The individual graphs and fits in the simulated vdM $x$-scan.
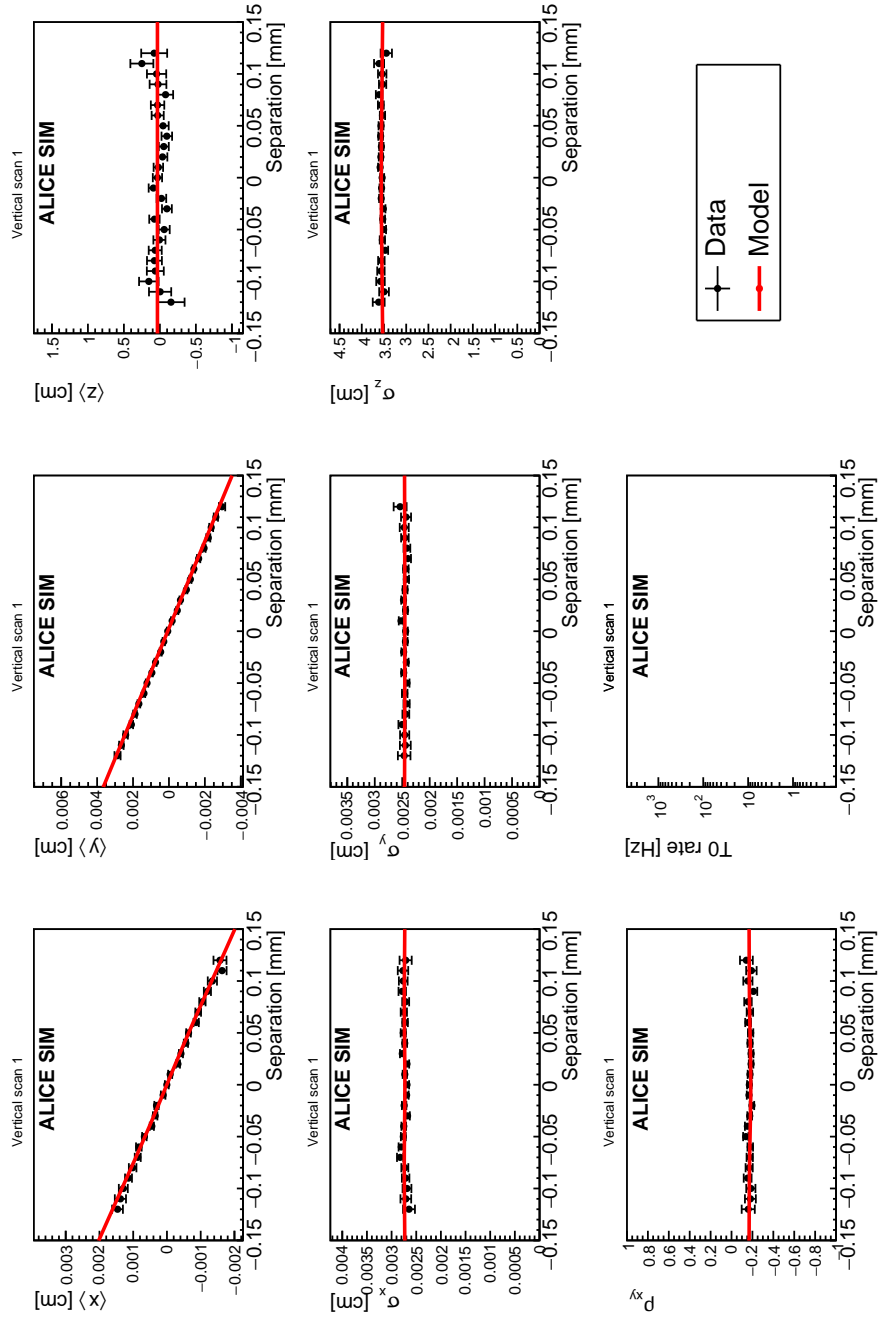
Figure A.12: The individual graphs and fits in the simulated vdM $y$-scan.

## Fitting double Gaussian bunches by single Gaussian model

The person performing the analysis should be very careful, because the single Gaussian model can describe data around head-on collisions, but it fails far away. The mean values can be fitted by 1st degree polynomial which is not enough as is shown in the following figures.

$\sigma_{1a}^X = 38.0 \pm 0.2$ μm                     $\sigma_{2a}^X = 31.2 \pm 0.1$ μm

$\sigma_{1a}^Y = 29.6 \pm 0.2$ μm                     $\sigma_{2a}^Y = 19.8 \pm 0.1$ μm

$\sigma_{1a}^Z = 7.3 \pm 0.0$ cm                       $\sigma_{2a}^Z = 7.3 \pm 0.0$ cm

$\rho_{1a}^{XY} = 0.09 \pm 0.01$                        $\rho_{2a}^{XY} = 0.07 \pm 0.01$

$\alpha^{XZ} = 0.0 \pm 0.0$ μrad

$\alpha^{YZ} = 0.0 \pm 0.0$ μrad

$R = 0.997_{-0.001}^{+0.001}$

$\chi^2/\text{NDF} = 431/327 = 1.3$

Figure A.13: The output parameters of the two double Gaussian bunches fitted by single Gaussian model. The input parameters were: $\sigma_{1a}^x = 39.7$ μm, $\sigma_{1a}^y = 26.5$ μm, $\rho_{1a}^{xy} = 0.26$, $\sigma_{1b}^x = 37.3$ μm, $\sigma_{1b}^y = 32.6$ μm, $\rho_{1b}^{xy} = -0.06$, $\sigma_{2a}^x = 36.6$ μm, $\sigma_{2a}^y = 23.5$ μm, $\rho_{2a}^{xy} = -0.05$, $\sigma_{1,2a}^z = 7.5$ cm, $\sigma_{2b}^x = 22.0$ μm, $\sigma_{2b}^y = 13.6$ μm, $\rho_{2a}^{xy} = 0.25$, $\sigma_{1b}^z = 7.1$ cm, $\sigma_{2b}^z = 7.0$ cm.
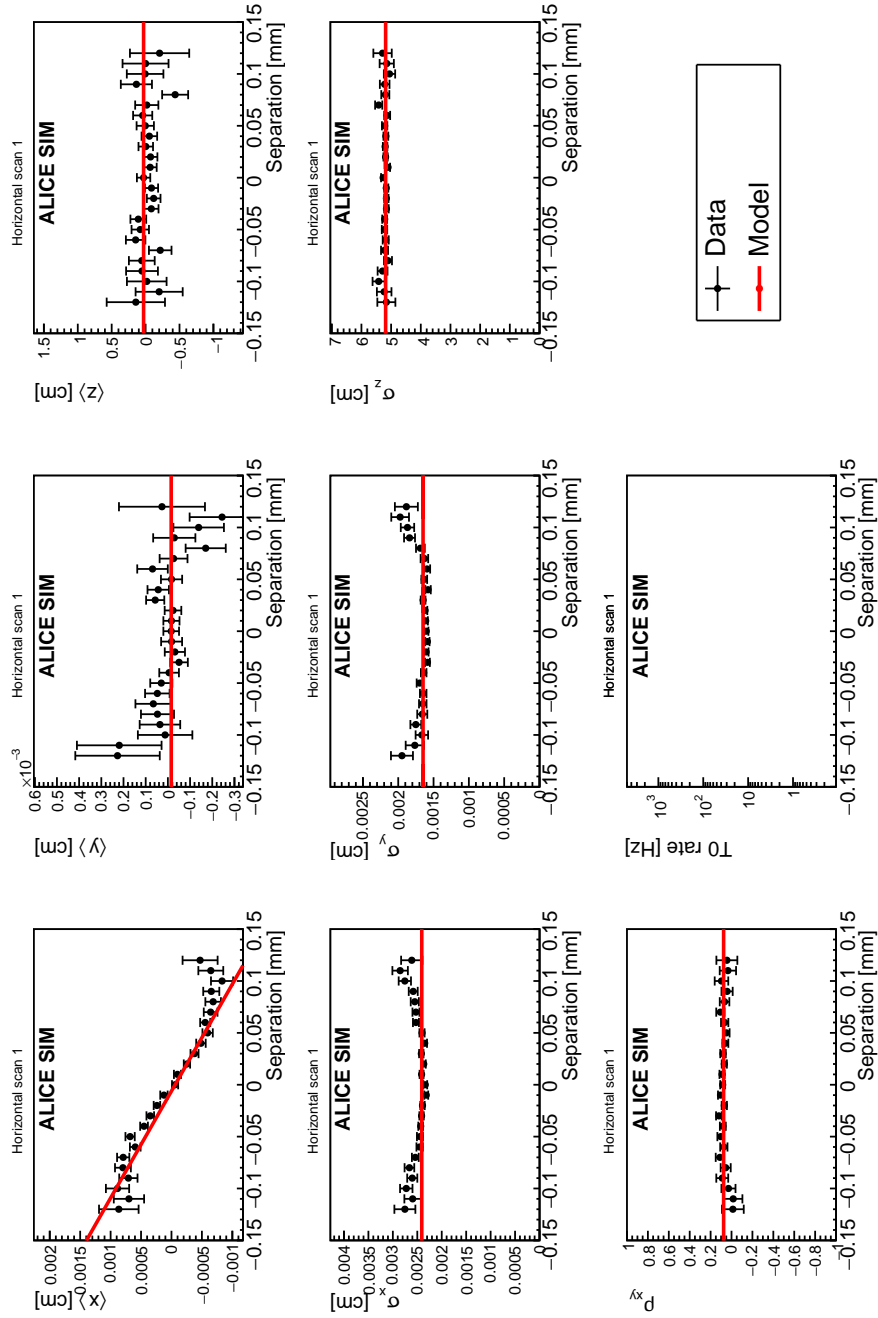
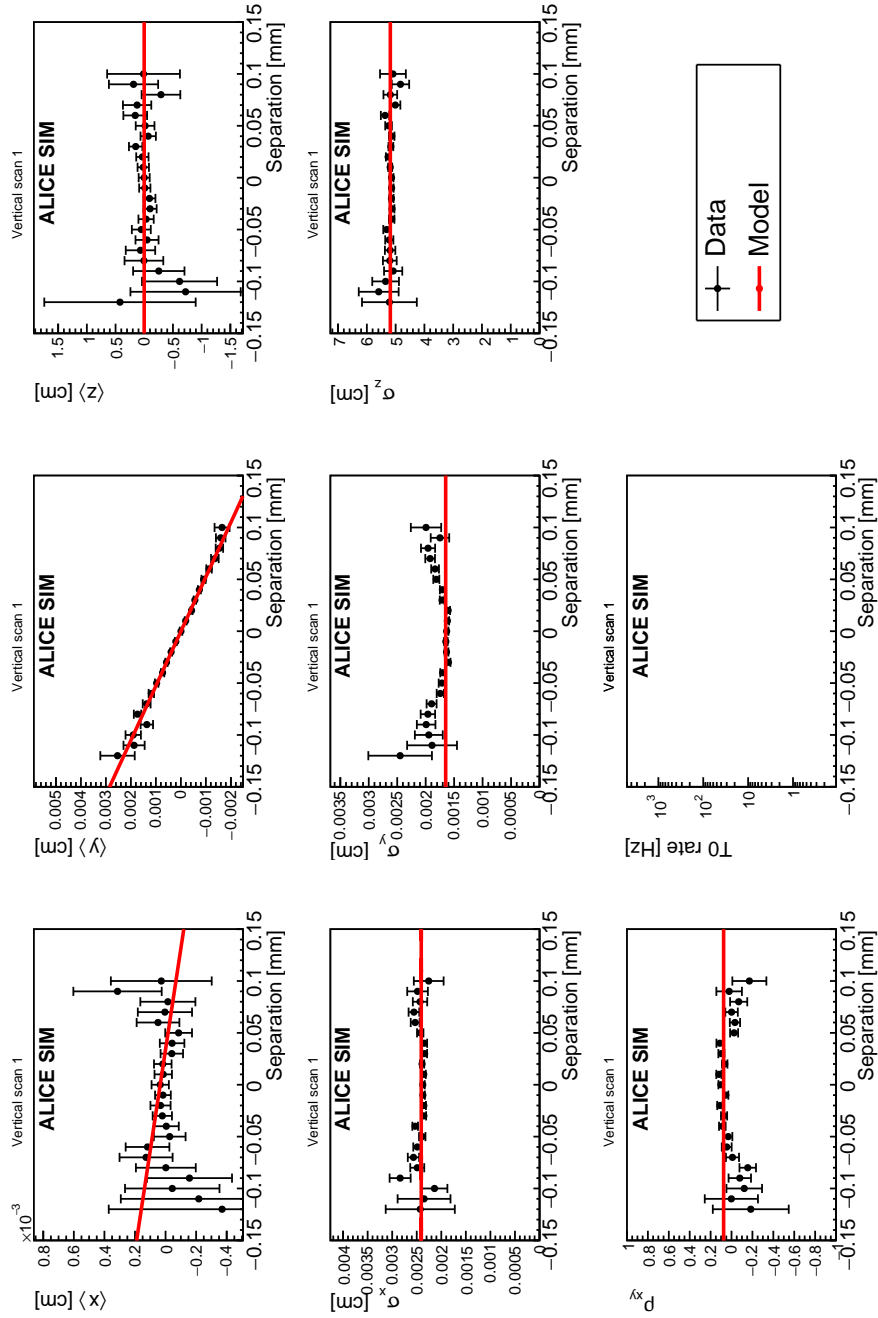Figure A.14: The individual graphs and fits in the simulated vdM $x$-scan.

Figure A.15: The individual graphs and fits in the simulated vdM $y$-scan.